Paleobiology

cambridge.org/pab

The evolution of femoral morphology in giant non-avian theropod dinosaurs

Romain Pintore[1,2], John R. Hutchinson[2], Peter J. Bishop[3,4], Henry P. Tsai[5] and Alexandra Houssaye[1]

[1]Mécanismes adaptatifs et évolution (MECADEV)/UMR 7179, CNRS/Muséum National d'Histoire Naturelle, Paris 75005, France
[2]Structure and Motion Laboratory, Royal Veterinary College, Hatfield AL9 7TA, U.K.
[3]Museum of Comparative Zoology and Department of Organismic and Evolutionary Biology, Harvard University, Cambridge, Massachusetts 02138, U.S.A.
[4]Geosciences Program, Queensland Museum, Brisbane, Queensland 4011, Australia
[5]Department of Biology, Southern Connecticut State University, New Haven, Connecticut 06515, U.S.A.

Article

Cite this article: Pintore R, Hutchinson JR, Bishop PJ, Tsai HP, Houssaye A (2024). The evolution of femoral morphology in giant non-avian theropod dinosaurs. *Paleobiology* **50**, 308–329. https://doi.org/10.1017/pab.2024.6

Received: 30 August 2023
Accepted: 16 February 2024

Corresponding author:
Romain Pintore;
Email: romain.pintore@edu.mnhn.fr

Non-technical Summary

Theropods are bipedal dinosaurs that appeared 230 million years ago and are still extant as birds. Their history is characterized by extreme variations in body mass, with gigantism evolving independently and on several occasions between many theropod groups. However, no study has shown whether all theropods evolved the same limb adaptations to high body mass or whether they had different morphologies. Here we studied the shape variation across 68 femora from 41 species of theropods using a 3D comparative approach, multivariate statistics, and phylogenetically informed analyses. We demonstrated that all the heaviest theropods evolved similar adaptations regardless of their phylogenetic affinities by enlarging muscular attachments and articular surfaces. We also highlighted that the lightest theropods evolved femoral adaptations to miniaturization, which occurred close to the bird lineage (Avialae). In addition, our results support a gradual evolution of known "avian" features, independent from body mass variations, which may relate to a more "avian" type of locomotion, where the knee drives hindlimb movement instead of the hip, like in earlier theropod relatives. The distinction between body mass variations and a more "avian" locomotion is represented by a decoupling in the mediodistal crest morphology, whose biomechanical nature should be studied to better understand the importance of its functional role in gigantism, miniaturization, and the evolution of a more "avian" type of locomotion.

Abstract

Theropods are obligate bipedal dinosaurs that appeared 230 Ma and are still extant as birds. Their history is characterized by extreme variations in body mass, with gigantism evolving convergently between many lineages. However, no quantification of hindlimb functional morphology has shown whether these body mass increases led to similar specializations between distinct lineages. Here we studied femoral shape variation across 41 species of theropods ($n = 68$ specimens) using a high-density 3D geometric morphometric approach. We demonstrated that the heaviest theropods evolved wider epiphyses and a more distally located fourth trochanter, as previously demonstrated in early archosaurs, along with an upturned femoral head and a mediodistal crest that extended proximally along the shaft. Phylogenetically informed analyses highlighted that these traits evolved convergently within six major theropod lineages, regardless of their maximum body mass. Conversely, the most gracile femora were distinct from the rest of the dataset, which we interpret as a femoral specialization to "miniaturization" evolving close to Avialae (bird lineage). Our results support a gradual evolution of known "avian" features, such as the fusion between lesser and greater trochanters and a reduction of the epiphyseal offset, independent from body mass variations, which may relate to a more "avian" type of locomotion (more knee than hip driven). The distinction between body mass variations and a more "avian" locomotion is represented by a decoupling in the mediodistal crest morphology, whose biomechanical nature should be studied to better understand the importance of its functional role in gigantism, miniaturization, and higher parasagittal abilities.

Introduction

Theropod dinosaurs first appeared in the Late Triassic and radiated in the Early Jurassic, before giving rise to birds (Ostrom 1976; Gatesy and Middleton 1997; Padian and Chiappe 1998; Holtz and Osmólska 2004; Brusatte et al. 2010; Irmis 2011; Benson 2018), one of the most diverse clades of extant vertebrates. Non-avian theropods are characterized by a strictly

bipedal locomotor habit and extreme body-size variations that ranged from a few grams to several tons, making them the largest terrestrial obligate bipeds ever (Sereno 1999; Carrano 2000, 2006; Farlow et al. 2000; Benson et al. 2014; Hutchinson 2021; D'Emic et al. 2023). Extreme theropod body-size increases appeared after the Triassic/Jurassic transition and followed a general trend toward gigantism that was common in several dinosaurian lineages (e.g., Theropoda, Sauropodomorpha, Thyreophora, Iguanodontia, Ceratopsidae) from the Early Jurassic to the Late Cretaceous, but also within Theropoda itself (Sereno 1999; Holtz and Osmólska 2004; Carrano 2006; Irmis 2011; Benson et al. 2014; Hutchinson 2021). Indeed, body mass increased convergently among several theropod lineages, reaching numerous occurrences of gigantism (Zanno and Makovicky 2013; Benson et al. 2014; Lee et al. 2014; Tsai et al. 2018, 2020; Cullen et al. 2020); usually defined as masses greater than 1000 kg (Sereno 1999; Benson et al. 2018; Cullen et al. 2020; Hutchinson 2021). More specifically, Benson et al. (2014) demonstrated that, out of 16 exceptional shifts (i.e., defined as shifts in evolutionary rates at nodes significantly differing from the overall pattern) in theropod body mass, 12 represented an increase. The remaining four occurrences of extreme shifts in body mass involved size decreases, with some linked to the miniaturization trend on the line to birds (Carrano 2006; Benson et al. 2014, 2018; Brusatte et al. 2014; Lee et al. 2014). This miniaturization seems to have paralleled the evolution of a more knee-driven locomotion closer to that of crown birds (Hutchinson and Gatesy 2000; Hutchinson and Allen 2009; Allen et al. 2021).

Inevitably, these changes of body mass are associated with changes in the morphology of hindlimb bones (Gregory 1912; Biewener 1983, 1989; Carrano 1998, 2001; Campione and Evans 2012; Mallet et al. 2019; Etienne et al. 2021). Archosaurian femoral morphology was highly constrained by several biological factors such as variations of body size/mass, shifts in locomotor habits, variation from a more sprawling to erect posture, and a shift from a more hip- to knee-driven gait, as demonstrated through morphometrics, biomechanics, microanatomy, and embryology (Charig 1972; Bakker and Galton 1974; Parrish 1986; Gatesy 1990; Christiansen 1998; Carrano 1999; Farlow et al. 2000; Hutchinson and Gatesy 2000; Maidment and Barrett 2012; Bishop et al. 2018a,b; Allen et al. 2021; Egawa et al. 2022; Lefebvre et al. 2022). The resulting shifts in the functional morphology and biomechanics of the femur have been investigated at the scale of Archosauria as a whole, but also between several dinosaurian clades and in the context of major faunal turnover across biological crises (Kubo and Kubo 2012; Sookias et al. 2012; Bishop et al. 2018a,b, 2020; Cuff et al. 2022; Pintore et al. 2022b). However, how the femoral anatomy evolved along with repeated body mass increases among theropods remains poorly studied despite the high number of convergences. Furthermore, theropods provide a singular opportunity to study how femora of obligate bipeds evolved specialization to gigantism without shifting to quadrupedal habits, as in all other clades, which evolved gigantism primarily as quadrupeds.

Here, we investigate femoral changes that occurred within Theropoda during variations of body mass and the evolution of a more knee-driven locomotor habit toward the avian line from the Late Triassic to the Late Cretaceous. We quantify the morphological variation of theropod femora using 3D geometric morphometrics (3D GMM), which is well-suited to infer aspects of the functional morphology of hindlimb bones from their shape in extant and extinct vertebrates (Martín-Serra et al. 2014; Hedrick et al. 2020; Lefebvre et al. 2020; Mallet et al. 2022; Pintore et al. 2022b). Following a similar approach among early archosauriform femora, Pintore et al. (2022b) demonstrated that the width of the epiphysis and the fourth trochanter position and shape were correlated to variations in body mass and independent from shifts in locomotor habits, as indicated by a decoupling in the fourth trochanter morphology between variations of body mass (i.e., more distally located in the heaviest taxa) and locomotor habits (i.e., proximo-distally symmetric in quadrupedal taxa and asymmetric with a steeper distal slope in bipedal taxa). In addition, features associated with body mass variations were demonstrated as evolving convergently between avemetatarsalians and pseudosuchians, whereas a high phylogenetic signal was recovered for features correlated to locomotor shifts. This finding sheds light on homoplastic features, which cladistic analyses desire to avoid. Therefore, we presume that features correlating with body mass variations in earlier archosauriforms would also vary convergently between the major theropod lineages included in our study, which independently evolved gigantism while remaining exclusively bipedal. Furthermore, the 3D GMM approach allows us to highlight several variations of commonly discussed femoral features relevant to theropod locomotion (e.g., proximo-distal shift of the fourth trochanter, offset of the femoral head, proximal extension of the lesser trochanter) and to test for their relationships with evolutionary allometry, phylogeny, and the evolutionary continuum from of more hip- to knee-driven type of locomotion within the lineage leading to extant birds. Investigating how femoral morphology accommodates convergent changes of body mass along with hindlimb orientation and more hip-/knee-driven locomotion in strictly bipedal animals is of major interest for understanding the extent of decoupling between morphological variations that are size related (homoplasy) versus those related to hindlimb orientation.

Materials and Methods

Sample

Our sample integrates 68 femora from 41 species of theropods, including 20 femora of specimens with an estimated body mass exceeding 1000 kg (which are hereby referred as "giants") following the body mass estimation function for bipedal dinosaurs based on the minimal diaphyseal circumference (MDC) from Campione et al. (2014; Table 1). The error range of body mass estimation was investigated by plotting a regression between log-transformed MDC and estimated body masses across all specimens from the sample (Supplementary Fig. S1). Specimens were selected to best document the multiple occurrences of gigantism across theropod phylogeny, within the constraint of availability and suitability for 3D surface digitization. We define our outgroup as all non-averostran theropods represented in our sample (*Coelophysis bauri* and *Liliensternus liliensterni* from the Late Triassic; *Dilophosaurus wetherilli* from the Early Jurassic; Fig. 1; Table 1). Ceratosauria is represented by several individuals from both Ceratosauridae and Abelisauroidea. Ceratosauridae includes two species of *Ceratosaurus*, the relatively small *C. nasicornis* and the more robust species *C. dentisulcatus* (body mass indicators are indicated in Table 1), which could be synonyms from different ontogenetic stages (Carrano and Sampson 2008; Carrano et al. 2012; Fig. 1). Our assemblage of Abelisauroidea is representative of the body-size range estimated within this clade by Grillo and Delcourt (2017), because it includes several specimens of one of

https://doi.org/10.1017/pab.2024.6 Published online by Cambridge University Press

Table 1. List of all femora included in this study. Estimated body masses were based on Campione et al. (2014; see details in "Materials and Methods" section) and integrated a 25% prediction error range. Abbreviations: BM, body mass (kg); CT, CT scan; Dig., digitization method; FL, femoral length (mm); L, left; MDC, minimal diaphyseal circumference (mm); Nb, number; Ph, photogrammetry; R, right; S, side; SS, surface scan. Known juveniles are highlighted with an asterisk (*) after the species name. Museo Nacional de Historia de Chile provided access to the *Chilesaurus* right femur of SNGM 1935. The file was downloaded from www.sketchfab.com; https://skfb.ly/6BsDo. The Smithsonian Institution provided access to the *Tyrannosaurus* right femur of PAL555000/MOR555. The file was downloaded from www.3d.si.edu; https://3d.si.edu/object/3d/tyrannosaurus-rex-osborn-1905-right-femur:17e443cb-7e7e-4634-b662-2057fea0aea1.

Higher order	Species	Abb.	Collection no.	S	FL	MDC	BM	Dig
Non-averostran Theropoda	*Coelophysis bauri*	Coe	UCMP 129618	R	252.7	62.7	18	SS
Non-averostran Theropoda	*Liliensternus liliensterni*	Lil	HMN BMR2175a	R	406.1	100.6	66	Ph
Non-averostran Theropoda	*Liliensternus liliensterni*	Lil	HMN BMR2175b	R	390.9	103.9	70	Ph
Non-averostran Theropoda	*Dilophosaurus wetherilli*	Dil	TMM 4324626	R	514.7	138.9	153	Ph
Non-averostran Theropoda	*Dilophosaurus wetherilli*	Dil	UCMP 37302	L	586.3	180.3	263	CT
Ceratosauria, Ceratosauroidae	*Ceratosaurus nasicornis*	Cer	BYUVP 765-4970	L	690.5	254.5	842	Ph
Ceratosauria, Ceratosauroidae	*Ceratosaurus nasicornis**	Cer	TPI 1010	R	412.2	146.3	172	Ph
Ceratosauria, Ceratosauroidae	*Ceratosaurus* indet.	Cer	UMNH VP5278	L	758.1	286.3	1052	CT
Ceratosauria, Abelisauroidae	*Masiakasaurus knopfleri*	Mas	FMNH PR2117	L	202.2	62.4	18	CT
Ceratosauria, Abelisauroidae	*Masiakasaurus knopfleri*	Mas	FMNH PR2153	R	195.6	61.4	17	CT
Ceratosauria, Abelisauroidae	*Masiakasaurus knopfleri*	Mas	UA 8684	L	196.3	66.9	21	CT
Ceratosauria, Abelisauroidae	Abelisaurid indet.	Abe	MPEF 10826	R	551.9	209.6	494	SS
Ceratosauria, Abelisauroidae	*Eoabelisaurus mefi*	Eao	MPEF 3990	L	614.5	241.5	730	SS
Ceratosauria, Abelisauroidae	*Skorpiovenator bustingorryi*	Sko	MMCH PV48	R	726.9	266.3	891	Ph
Ceratosauria, Abelisauroidae	*Carnotaurus sastrei*	Car	MACN 894	L	988.8	320.1	1584	Ph
Tetanurae, indet.	*Chilesaurus diegosuarezi**	Chi	SNGM 1935	R	131.8	56.6	14	SS
Tetanurae, Megalosauroidae	*Piatnitzkysaurus floresi*	Pia	MACN CH895	L	573.4	207.3	472	Ph
Tetanurae, Megalosauroidae	*Torvosaurus tanneri*	Tor	GPM 0012.01	R	804.3	371.9	2355	Ph
Tetanurae, Megalosauroidae	*Torvosaurus tanneri*	Tor	GPM 0012.02	L	815.9	365.3	2293	Ph
Tetanurae, Megalosauroidae	*Spinosaurus aegyptiacus*	Spi	FSAC KK11888	L	604.5	236.8	673	CT
Tetanurae, Megalosauroidae	*Suchomimus tenerensis*	Suc	MNBH GAD500	L	1061.9	393.3	2680	CT
Tetanurae, Allosauroidae	*Erectopus superbus*	Ere	MNHN 2001-4	L	452.4	174.1	299	SS
Tetanurae, Allosauroidae	*Tyrannotitan chubutensis*	Tyr	MPEF 1157	R	1296.5	530.8	5935	Ph
Tetanurae, Allosauroidae	*Giganotosaurus carolinii*	Gig	MUCPv Ch1	L	1374.4	518.4	5961	Ph
Tetanurae, Allosauroidae	*Allosaurus fragilis*	All	UMNH VP7884	L	700.3	259.9	899	CT
Tetanurae, Allosauroidae	*Allosaurus fragilis*	All	UMNH VP7885	R	571.1	210.6	452	CT
Tetanurae, Allosauroidae	*Allosaurus* indet.	All	TATE V3587	R	773	318.2	1497	Ph
Tetanurae, Allosauroidae	*Allosaurus* indet.	All	TATE V6775	L	758.2	286.5	1054	Ph
Tetanurae, Allosauroidae	*Allosaurus jimmadseni*	All	MOR 693	L	734.5	266.2	961	CT
Tetanurae, Allosauroidae	*Allosaurus jimmadseni*	All	MOR 693	R	751.2	279.5	1099	CT
Tetanurae, Tyrannosauroidae	*Guanlong wucaii*	Gua	IVPP V14531	L	394.8	84.1	40	SS
Tetanurae, Tyrannosauroidae	*Gorgosaurus libratus*	Gor	TMP 1994.012.0602	R	904.3	330.7	1744	CT
Tetanurae, Tyrannosauroidae	*Alioramus altai*	Ali	IGM 100 1844	L	542.4	170.7	281	Ph
Tetanurae, Tyrannosauroidae	*Teratophoneus curriei*	Ter	UMNH VP16690	L	559.9	214.9	533	CT
Tetanurae, Tyrannosauroidae	*Teratophoneus curriei*	Ter	RAM 9132	R	786	269.4	971	Ph
Tetanurae, Tyrannosauroidae	*Daspletosaurus torosus*	Das	TMP 2001.036.0001	R	949.4	379.9	2497	CT
Tetanurae, Tyrannosauroidae	*Tarbosaurus bataar**	Tar	ZPAL MgD-I/175	L	753.1	300.8	1314	Ph
Tetanurae, Tyrannosauroidae	*Tyrannosaurus rex*	Trx	MOR 555	R	1275.4	531.2	6366	SS
Tetanurae, Tyrannosauroidae	*Tyrannosaurus rex*	Trx	MOR 1125	L	1139.4	522.2	5987	CT
Tetanurae, Tyrannosauroidae	*Tyrannosaurus rex*	Trx	MOR 1128	L	1215.4	591.1	7978	CT

(*Continued*)

https://doi.org/10.1017/pab.2024.6 Published online by Cambridge University Press

Table 1. (*Continued.*)

Higher order	Species	Abb.	Collection no.	S	FL	MDC	BM	Dig
Tetanurae, Tyrannosauroidae	*Tyrannosaurus rex*	Trx	CM 9380	R	1243.3	577.8	7907	SS
Tetanurae, Tyrannosauroidae	*Tyrannosaurus rex*	Trx	TMM 40811	R	1006.7	585.7	8395	SS
Tetanurae, Tyrannosauroidae	*Tyrannosaurus rex*	Trx	FMNH PR2081	L	1349.4	595.5	8728	SS
Tetanurae, Ornithomimosauria	Ornithomimidae indet.	Orn	ANG 10 90	L	349.2	108.7	81	SS
Tetanurae, Ornithomimosauria	Ornithomimidae indet.	Orn	ANG 15 3865	R	378.7	102.3	58	SS
Tetanurae, Ornithomimosauria	Ornithomimidae indet.	Orn	ANG 16 5120	R	343.4	103.8	72	SS
Tetanurae, Ornithomimosauria	*Gallimimus bullatus*	Gal	ZPAL MgD-1 8	R	604.7	165.8	249	Ph
Tetanurae, Ornithomimosauria	*Gallimimus bullatus*	Gal	ZPAL MgD-1 1	R	345.7	104.2	68	Ph
Tetanurae, Ornithomimosauria	*Gallimimus bullatus*	Gal	ZPAL MgD-1 94	L	258.1	72.5	27	Ph
Tetanurae, Therizinosauria	*Falcarius utahensis*	Fal	NCSM 28007	L	240.9	70.8	25	SS
Tetanurae, Therizinosauria	*Falcarius utahensis*	Fal	UMNH VP12361	R	318.5	116.2	95	Ph
Tetanurae, Therizinosauria	*Falcarius utahensis*	Fal	NCSM 26199	R	291.9	92.9	53	SS
Tetanurae, Therizinosauria	*Nothronychus graffami*	Not	UMNH VP16420	R	682.5	306.9	1046	CT
Tetanurae, Oviraptorosauria	*Caenagnathus collinsi*	Cae	TMP 1986.036.0323	R	351.2	110.3	85	CT
Tetanurae, Oviraptorosauria	*Anzu wyliei*	Anz	CM 78000	R	515.2	165.9	243	Ph
Tetanurae, Oviraptorosauria	*Anzu wyliei*	Anz	CM 78001	R	484.6	141.5	161	Ph
Tetanurae, Oviraptorosauria	*Citipati osmolskae*	Cit	IGM 100-978	L	338.1	121.1	110	Ph
Tetanurae, Oviraptorosauria	*Conchoraptor gracilis*	Con	AMNH 30880	R	142.4	55.1	13	Ph
Tetanurae, Dromaeosauridae	*Bambiraptor feinbergi*	Bam	FIP 001	L	117.5	31.9	3	SS
Tetanurae, Dromaeosauridae	*Bambiraptor feinbergi*	Bam	FIP 001	R	113.1	32.5	3	SS
Tetanurae, Dromaeosauridae	*Deinonychus antirrhopus*	Dei	MCZ VPRA-4371	L	334.9	117.8	100	Ph
Tetanurae, Dromaeosauridae	*Velociraptor mongoliensis*	Vel	IGM 10 986	L	181.6	61.4	17	SS
Tetanurae, Dromaeosauridae	*Utahraptor ostrommaysi*	Uta	BYUVP 7510-18078	R	530.8	247.2	777	Ph
Tetanurae, Dromaeosauridae	*Utahraptor ostrommaysi*	Uta	BYUVP 2586	L	481.3	198.1	391	Ph
Tetanurae, Dromaeosauridae	*Utahraptor ostrommaysi*	Uta	BYUVP 1833	R	573.5	215.4	481	Ph
Tetanurae, Troodontidae	*Sinovenator changii*	Sin	IVPP V12615	R	117.7	32.4	3	SS
Tetanurae, Troodontidae	Troodontidae	Tro	MOR 553s -7.28.91.239	R	256.1	81.3	37	CT
Tetanurae, Troodontidae	Troodontidae	Tro	MOR 748	R	294.8	85.7	43	CT

the smallest noasaurids, *Masiakasaurus knopfleri*, the large abelisaurid *Carnotaurus sastrei*, and a specimen from Argentina, currently under description, similar to *Eoabelisaurus mefi* and *Skorpiovenator bustingorryi*, which are also included in our study (Fig. 1; Table 1). Early Tetanurae are represented by a juvenile individual of the bizarre, herbivorous *Chilesaurus diegosuarezi* (Novas et al. 2015), also hypothesized to represent the earliest-diverging ornithischian (Baron and Barrett 2017; Fig. 1; Table 1). Other tetanurans includes several specimens of Megalosauroidea, Allosauroidea, Tyrannosauroidea, Ornithomimidae, Therizinosauridae, Oviraptorosauridae, and paravians (Fig. 1; Table 1). Megalosauroidea are represented by *Piatnitzkysaurus floresi* from the Early Jurassic and *Torvosaurus tanneri* from the Late Jurassic (Fig. 1; Table 1). Megalosauroidea also includes two large Spinosauridae that each preserve a complete femur: *Suchomimus tenerensis* and *Spinosaurus aegyptiacus*, which may or may not have shared the same ecological (e.g., semi-aquatic) habits (Amiot et al. 2010; Ibrahim et al. 2014, 2020; Hone and Holtz 2021; Fabbri et al. 2022; Sereno et al. 2022; Fig. 1; Table 1). Early Allosauroidea comprises *Erectopus superbus*, which may be an early metriacanthosaurid or an allosaurid (Allain 2005; Carrano et al. 2012; Fig. 1; Table 1). Later allosaurids comprise *Allosaurus fragilis*, *A. jimmadseni*, and an indeterminate specimen from the Late Jurassic of the Morrison Formation informally referred to as "Wyomingraptor," which is relatively robust for the clade (Fig. 1; Table 1). Allosauridae's sister group Carcharodontosauridae includes the giant taxa *Tyrannotitan chubutensis* and *Giganotosaurus carolinii* (Fig. 1; Table 1). We include the proceratosaurid *Guanlong wucaii* as a small early-diverging tyrannosauroid (Fig. 1; Table 1). Tyrannosauridae comprises the albertosaurine *Gorgosaurus libratus*, the relatively small tyrannosaurine *Alioramus altai*, and its larger relatives *Teratophoneus curriei*, *Daspletosaurus torosus*, a juvenile *Tarbosaurus bataar*, and six specimens of *Tyrannosaurus rex* (Brusatte and Carr 2016; Fig. 1; Table 1). Ornithomimosauria are represented by an assemblage of an undescribed early Ornithomimidae from the Early Cretaceous of Angeac-Charente (France; Allain et al. 2014) and *Gallimimus bullatus*, a later relative of approximately the same size (Fig. 1; Table 1). Ornithomimosauria is the only major

https://doi.org/10.1017/pab.2024.6 Published online by Cambridge University Press

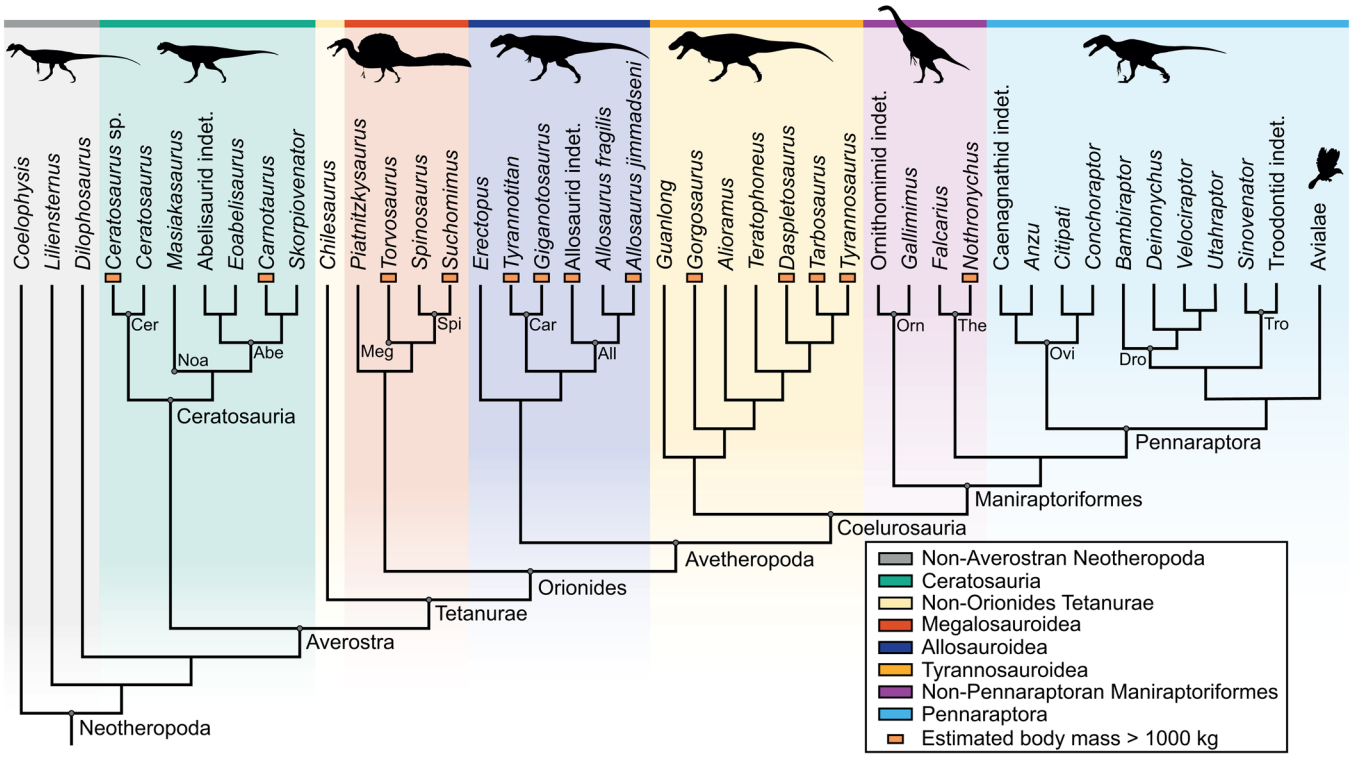

Figure 1. Phylogenetic tree of the theropods studied, based on Carrano and Sampson (2008), Carrano et al. (2012), Brusatte and Carr (2016), Zanno and Makovicky (2013), Turner et al. (2012), Novas et al. (2015), and Funston (2020). Silhouettes are from S. Hartman. Specimens with an estimated body mass greater than 1000 kg are highlighted with an orange rectangle. Abbreviations: Abe, Abelisauroidae; All, Allosauroidea; Car, Carcharodontosauridae; Cer, Ceratosauridae; Dro, Dromaeosauridae; Meg, Megalosauroidea; Noa, Noasauridae; Orn, Ornithomimidae; Ovi, Oviraptosauria; Spi, Spinosauroidea; The, Therizinosauridae; Tro, Troodontidae.

theropod clade that evolved gigantism (>1000 kg) for which we could not obtain representatives, such as deinocheirids. Therizinosauria comprises several specimens of *Falcarius utahensis*, an early representative of the clade, and one specimen of the larger therizinosaurid *Nothronychus graffami* (Fig. 1; Table 1). Oviraptosaurians are represented by both Caenagnathidae and Oviraptoridae (Fig. 1; Table 1). Oviraptorids include the heyuannian *Conchoraptor gracilis* and the relatively larger Citipatiinae *Citipati osmolskae*, represented here by the largest individual known for this species (Clark et al. 2001). Caenagnathidae comprises an indeterminate species of *Caenagnathus* and its relatively larger relative *Anzu wyliei*. Paravians are represented by the small troodontids *Sinovenator changii* and an indeterminate species (Fig. 1; Table 1). Paravians also include Dromaeosauridae with a range of body sizes spanning from the small *Bambiraptor feinbergi* and *Velociraptor mongoliensis* to the middle-sized *Deinonychus antirrhopus* and several specimens of the relatively large *Utahraptor ostrommaysi* (Fig. 1; Table 1). When available, well-preserved left and right femora from the same specimens were used (3 out of 65 individuals).

Taphonomic alterations have been demonstrated to affect the results of geometric morphometric and statistical analyses (Hedrick et al. 2019; Lefebvre et al. 2020; Wynd et al. 2021, Pintore et al. 2022a). Following results from Pintore et al. (2022a), we included only complete femora without visible distortion of the anteroposterior and lateromedial curvature of the diaphysis, as these types of deformations were demonstrated to have the greatest impact on 3D GMM analyses conducted on asymmetrical objects such as femora. The whole femur of *Nothronychus* (giant Therizinosauridae) is taphonomically flattened anteroposteriorly but preserves the relative proportions of condyles and trochanters. This type of affine deformation was documented as only having a slight effect on spline deformations in 3D GMM (Pintore et al. 2022a). Therefore, we chose to integrate it into our dataset to ensure representativeness of giant Therizinosauridae and to test for biological variations linked to an anteroposterior flattening of the femur in our results. Known ontogenetic stages are shown in Table 1.

Institutional Abbreviations. **AMNH**: American National History Museum, New York, NY, USA; **ANG**: Angeac-Charente Collection, Musée d'Angoulême, Angoulême, France; **BYU**: Brigham Young University Museum of Paleontology, Provo, UT, USA; **CM**: Carnegie Museum of Natural History, Pittsburgh, PA, USA; **FIP**: Florida Institute of Paleontology, Wellington, FL, USA; **FMNH**: Field Museum of Natural History, Chicago, IL, USA; **FSAC**: Faculté des Sciences Aïn Chock, Casablanca, Morocco; **GPM**: Glenrock Paleontological Museum, Glenrock, WY, USA; **HMN**: Museum für Naturkunde, Berlin, Germany; **IGM**: Mongolian Geological Institute, Ulaanbaatar, Mongolia; **IVPP**: Institute of Vertebrate Paleontology and Paleoanthropology, Beijing, China; **MACN**: Museo Argentino de Ciencias Naturales Bernardino Rivadavia, Buenos Aires, Argentina; **MMCH**: Museo Paleontológico Municipal Ernesto Bachmann, Villa El Chocón, Argentina; **MNBH**: Musée National Boubou-Hama, Niamey, Niger; **MNHN**: Muséum National d'Histoire Naturelle, Paris, France; **MCZ VPRA**: Vertebrate Paleontology (Reptiles and

https://doi.org/10.1017/pab.2024.6 Published online by Cambridge University Press

Amphibians) Collection, Museum of Comparative Zoology, Harvard University, Cambridge, MA, USA; **MOR**: Museum of the Rockies, Bozeman, MT, USA; **MPEF**: Museo Paleontológico Egidio Feruglio, Trelew, Argentina; **MUCP**: Museo de la Universidad Nacional del Comahue, Neuquén, Argentina; **NCSM**: North Carolina Museum of Natural Sciences, Raleigh, NC, USA; **RAM**: Raymond M. Alf Museum of Paleontology, Claremont, CA, USA; **SNGM**: Servicio Nacional de Geología y Minería, Santiago, Chile; **TATE**: Tate Museum, Casper College, Casper, WY, USA; **TMM**: Jackson School of Geosciences Vertebrate Paleontology Laboratory, University of Texas, Austin, TX, USA; **TMP**: Royal Tyrrell Museum of Palaeontology, Drumheller, Canada; **TPI**: North American Museum of Ancient Life, Lehi, UT, USA; **UA**: Université d'Antananarivo, Antananarivo, Madagascar; **UCMP**: University of California Museum of Paleontology, Berkeley, CA, USA; **UMNH**: Utah Museum of Natural History, Salt Lake City, UT, USA; **ZPAL**: Institute of Paleobiology of the Polish Academy of Sciences, Warsaw, Poland.

3D Digitization

Various digitization approaches were used to create the 3D models (Table 1). The surface scanners Next Engine (NextEngine Inc., Santa Monica, CA, USA), Artec EVA and Space Spider (Artec 3D, Luxembourg), and Polhemus FastSCAN (Polhemus, Inc., Colchester, VT, USA) were used with their respective software for surface reconstructions (19 out of 68 femora): ScanStudio Pro (NextEngine Inc., Santa Monica, CA, USA) and Artec Studio Professional (Artec 3D, Luxembourg). Photogrammetry was performed using a Sony DSC-F828 (29 out of 68). Surface reconstructions were conducted using the package Bundler,[*] PMVS (Patch-based Multi-view Stereo Software),[**] Metashape Professional (Agisoft LLC, Russia), and Meshlab (Cignoni et al. 2008) to compute dense point clouds, create scaled 3D meshes, and mirror all the left femora. CT scans were segmented using Mimics (Materialise NV, Belgium) and Avizo (Thermo Fisher Scientific Inc., MA, USA) software to create 3D meshes (20 out of 68; see scan parameters in Supplementary Table S1). Several studies have demonstrated that the difference in the geometry of the resulting 3D morphologies was low when comparing photogrammetry, CT scans, and surfaces scans, especially when analyzing specimens at a large comparative scale (Falkingham 2012; Fau et al. 2016; Soodmand et al. 2018; Díez Díaz et al. 2021). Furthermore, Waltenberger et al. (2021) demonstrated that 3D GMM could properly analyze combined 3D models digitized from various approaches.

Geometric Morphometrics

We used 3D GMM to investigate the morphological variation within our dataset. This method relies on the digitization of anatomically (or geometrically) homologous landmarks (Zelditch et al. 2012). We digitized single anatomical landmarks and sliding semilandmarks along curves and surfaces following the protocol described in Gunz et al. (2005), Gunz and Mitteroecker (2013), and Botton-Divet et al. (2016). High-density 3D GMM is more effective than using anatomical landmarks alone to capture the entire morphology of biological objects and precisely describe shape variations, which is particularly useful, for example, to circumvent the lack of anatomical landmarks along the diaphysis of long bones (Gunz et al. 2009; Zelditch et al. 2012; Gunz and Mitteroecker 2013; Botton-Divet et al. 2015; Goswami et al. 2019).

In total, 662 landmarks, including 27 anatomical single landmarks, 163 sliding semilandmarks along curves, and 472 along surfaces, were used to measure the femoral variation across our dataset. We manually digitized anatomical landmarks and sliding semilandmarks along curves only on every specimen using the Landmark software v. 3.0.0.6 (Wiley et al. 2005). To minimize the impact of taphonomically eroded structures, we relied on concavities rather than convexities (e.g., borders rather than the tip of tuberosities; Supplementary Table S2). Unfortunately, we could not digitize landmarks along all key structures relevant to theropod locomotor functional morphology and biomechanics, because their borders were not clearly visible throughout the entirety of the specimens included in this study. For example, the trochanteric crest, on which the iliofemoralis externus (IFE) is thought to have inserted, was strongly reduced in Tetanurae (Hutchinson 2001) and therefore could not be included in our 3D GMM protocol. Additionally, we digitized the entirety of landmarks and semilandmarks (surfaces included) on one specimen hereby referred as "the template." We chose the femur of *Tyrannosaurus rex* FMNH PR2081, as it represents one of the best preserved specimens (i.e., with the most prominent structures of our dataset), ensuring that sliding semilandmarks will be correctly projected along the surfaces of every other specimen (Fig. 2). The projection was performed semi-automatically using the function *placePatch* of the R package Morpho v. 2.8 (Schlager 2017). Then, we performed two sets of spline relaxations minimizing the bending energy of a thin plate spline: (1) five iterations between the configurations of the template and every other specimen using the function *relaxLM* of Morpho; and (2) three iterations between a mean configuration and every specimen using the function *slideLM*. A more detailed workflow is presented in Pintore et al. (2022b). These steps ensured that all corresponding semilandmark coordinates were geometrically homologous between each specimen (Gunz et al. 2005). We performed a generalized Procrustes analysis (GPA) using the *gpagen* function from geomorph v. 3.3.1 (Adams and Otárola-Castillo 2013). GPA enables superimposition of every specimen in order to homogenize their positions in the Cartesian coordinate system and isolate the shape from the size component (Gower 1975; Rohlf and Slice 1990; Zelditch et al. 2012). The remaining differences between superimposed configurations (i.e., Procrustes residuals) could then be interpreted as the shape variation between all specimens.

We computed a principal component analysis (PCA) to reduce dimensionalities of the variation and isolate several morphological components (Gunz and Mitteroecker 2013). We also computed neighbor-joining trees using the total PCA scores to represent global morphological distances between each bone. Trees were computed in unrooted type based on Euclidean distances using the *distance*, *nj*, and *plot.phylo* functions of the ape R package (Paradis et al. 2004). Then, we computed regressions between PC axes and log-transformed estimated body masses to investigate whether one of these morphological components would highlight shape variations linked with body mass increase (Table 1). We performed repeatability testing by digitizing the same landmark configuration 10 times on three *Tyrannosaurus* femora (i.e., FMNH PR2081, TMM 40811, MOR 1125), which was the taxon with some of the least intraspecific variability between specimens from our dataset (Table 1). After computing a GPA and a

[*] http://www.cs.cornell.edu/~snavely/bundler.
[**] http://www.di.ens.fr/pmvs.

https://doi.org/10.1017/pab.2024.6 Published online by Cambridge University Press

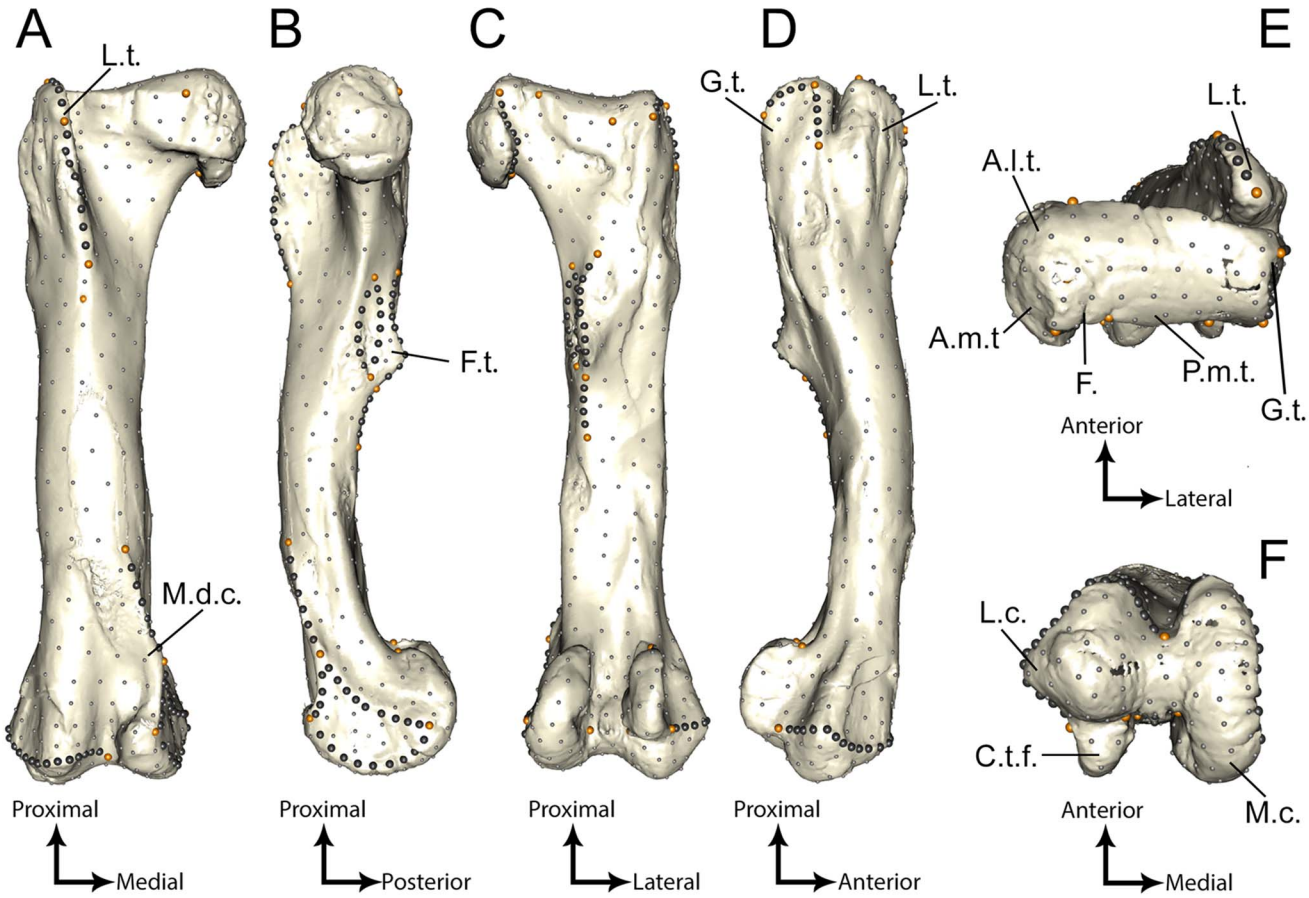

Figure 2. The template right femur of *Tyrannosaurus rex* (FMNH PR2081) with anatomical landmarks (orange) and sliding semilandmarks along curves (dark gray) and surface (light gray) in (A) anterior, (B) medial, (C) posterior, (D) lateral, (E) proximal, and (F) distal views. Abbreviations: A.l.t., anterolateral tuber; A.m.t., anteromedial tuber; C.t.f., crista tibiofibularis; F., fovea capitis; F.t., fourth trochanter; G.t., greater trochanter; L.c., lateral condyle; L.t., lesser trochanter; M.d.c, mediodistal crest; M.c., medial condyle; P.m.t., posteromedial tuber.

PCA, we highlighted three distinct clusters corresponding to the three different specimens, each composed of the 10 iterations of the same landmark configurations (Supplementary Fig. S2). This demonstrated that our landmark configuration was repeatable, because the biological variation was greater than the possible operator bias in reproducing the same landmark configuration multiple times on the same specimen. Once we identified the PC axis that polarized variations related to body mass increases, we computed 3D visualizations in order to highlight the associated femoral features. To do so, we calculated a mean shape between all the femora of our dataset by performing a spline relaxation between the template landmark configuration and a mean landmark configuration extracted from the GPA. The associated TPS deformation was used to warp the template mesh onto the mean landmark configuration in order to create the mean shape of all the specimens. From this step, we could interpolate the mean landmark configuration with the configurations at the most negative and positive extremes of the chosen PC axis in order to create minimal and maximal theoretical shapes. To further highlight which features varied the most, we computed vectors of displacement between every landmark and semilandmark of the two extreme morphologies using the function *segments3d* of the rgl R package v. 0.100.54 (Adler and Murdoch 2020) that we colored with a heat-map gradient using the *blue2red* functions of the ColorRamps R package (Keitt 2008; Botton-Divet 2017).

The allometric effect (i.e., evolutionary and ontogenetic allometry; Klingenberg 2016) was analyzed using different sets of metrics (Table 1). We measured the femoral lengths (FL; i.e., maximal height of the proximal end relative to the distal end) across all our specimens using Meshlab v. 2020.06 (Cignoni et al. 2008). Campione and Evans (2012, 2020) demonstrated that the MDC of the femur was a reliable indicator of body mass (BM) in dinosaurs. We thus extracted MDC using the Cross Section and Extract Contours tools of the software CloudCompare v. 2.12.[***] We computed more precise estimations of BM following the methodology provided by (Campione et al. 2014), which was developed specifically for the femur of bipedal non-avian dinosaurs, using the function *bipeds* from the R package MASSTIMATE v. 2.0 (Campione 2016). The equation relies on MDC, and the output is corrected by an index ("cQE.cor" in the *bipeds* function) based on the eccentricity at the MDC of the femur, which we measured using Meshlab v. 2020.06 (Cignoni et al. 2008). We also investigated the size effect within our dataset by computing Pearson's correlation tests between

[***]https://www.cloudcompare.org/.

https://doi.org/10.1017/pab.2024.6 Published online by Cambridge University Press

the log-transformed centroid size and estimated body masses of each specimen and their distribution along the chosen PC axis using the R function *cor.test*, for which a significant result would indicate that shape variation along that axis had an allometric component (Mitteroecker and Gunz 2009).

We constructed a phylogeny following Carrano and Sampson (2008), Carrano et al. (2012), Brusatte and Carr (2016), Zanno and Makovicky (2013), Turner et al. (2012), Novas et al. (2015), and Funston (2020) using Mesquite software v. 3.6.1 (Maddison and Maddison 2019) with all branch lengths set to one (Fig. 1). We mapped this phylogeny onto the PCA in order to compute a phylomorphospace using the function *plot.gm.prcomp* of the geomorph package. We used the K_{mult} statistics, an extension of Blomberg's *K* (Blomberg et al. 2003), to quantify how much the constructed phylogeny compares with its expectation under a Brownian motion model based on the distribution of specimens in the complete morphospace and along chosen PC axes (Adams 2014a). When significant, the K_{mult} statistics indicates a relationship between phylogeny and the variation of femoral morphology. A value below one would indicate that the phylogeny did not predict the variation of femoral morphology under a Brownian model of evolution well enough, likely suggesting convergence, whereas a value equal to or above one would suggest variation between clades and according to the phylogeny (i.e., phylogenetic signal). In addition, we conducted phylogenetic generalized least squares regressions (PGLS) to investigate the covariation between our different size metrics and the femoral morphology while accounting for phylogenetic relationships under Brownian motion across our theropod dataset at the unidimensional (i.e., along one isolated PC axis) and multidimensional (i.e., across all PC axes) levels (Adams 2014b).

To assess branch length sensitivity over our phylogenetically based statistical analyses (i.e., phylogenetic signal and PGLS), we compared results obtained from a time-calibrated tree (with real and transformed branch lengths) with our results obtained from our phylogeny with equal branch lengths (Supplementary Material). The time-calibrated tree was created based on the minimal and maximal known ages from each taxon in our sample. We used the R package paleotree (Bapst 2014) to optimize date ranges per taxon in branch lengths and to estimate node dates from these time ranges using the *dateNodes* function, which provided the time-calibrated tree with "real" branch lengths. We then reran the analyses on the time-calibrated tree following the same protocol as described earlier. The sensitivity analyses yielded similar results when investigating phylogenetic signal and evolutionary allometry using equal and real branch lengths (Supplementary Material). Therefore, we favored using equal branch lengths over "real" branch lengths, as the latter represented a greater assumption, given that our sample is phylogenetically large and composed of fossils with uncertainty regarding their ages (Supplementary Material).

Results

Morphological Variation

First, we investigated the global morphological variation using the neighbor-joining tree (Supplementary Fig. S3). This visualization highlights that specimens from the same species are consistently clustered together but that clades seem spread across the neighbor-joining tree (Supplementary Fig. S3). This observation is consistent with the distribution of specimens along the first axis of the PCA (PC 1; Fig. 3A). The first two axes of the PCA (PC 1 and PC 2) represent more than 50% of the global morphological variation (40.0% and 11.3%, respectively; Fig. 3A). PC 1 represents essentially femoral robusticity (i.e., epiphyseal width relative to the diaphyseal length; Figs. 3, 4A), whereas PC 2 broadly represents the degree of fusion of trochanters and curvature of various femoral features (Figs. 3, 4B).

The distribution of the specimens along the first axis follows an increase of body mass, as shown by the increase of the circle size toward the positive side (Fig. 3A) and its significant association with log-transformed centroid size (see details in "Evolutionary Allometry"). Indeed, every specimen with a body mass estimation > 1000 kg is located on the positive side of PC 1, except the large abelisaurid *Carnotaurus* (Fig. 3A; Car). All early non-averostran neotheropods and maniraptoriforms (i.e., pennaraptoran and non-pennaraptoran maniraptoriforms) are located on the negative side of PC 1 (except the giant therizinosaurid *Nothronychus*, the relatively large dromaeosaurid *Utahraptor*, and, surprisingly, the smallest of our oviraptosaurids, *Conchoraptor*; Figs. 3A, 5; Not, Con). All troodontids and the ~2 kg dromeosaurid *Bambiraptor* form a cluster together on the most negative extreme of PC 1 and are clearly isolated from the rest of the sample (Figs. 3A, 5; Bam, Sin, Tro). All specimens of Tetanurae, other than maniraptoriforms (i.e., *Chilesaurus*; allosauroids; megalosauroids, except the early *Erectopus*; and tyrannosauroids, except the smallest taxa *Guanlong* and *Alioramus*), are located on the positive side of PC 1 (Fig. 3A; Chi, Ere, Gua, Ali). Ceratosaurs are located close to the center of PC 1, with the smallest (*Masiakasaurus*) and the largest (*Carnotaurus*) taxa having negative values and the other, medium-sized taxa, having positive values (Fig. 3A; Mas, Car).

Theoretical shapes and vectors displaying the amount of landmark displacement highlight that the most important morphological variation is located on the distal ridge of the fourth trochanter (Fig. 4A). The ridge is also more prominent and proximo-distally wider on the maximal theoretical shape, whereas it is flatter and proximal-distally narrower on the minimal theoretical shape (Figs. 3B, 4A). The distribution along PC 1 also varies according to the epiphyseal width relative to the diaphyseal length (i.e., femoral robusticity; Fig. 3B,D,E). In the proximal epiphysis, the longest vectors are on the medial side of the femoral head, which is upturned on robust femora and downturned on gracile ones (Fig. 4A). In the distal epiphysis, the longest vectors are on the anterior part of the mediodistal crest, which is greatly proximodistally enlarged toward the middle of the shaft in the most robust femora (Fig. 4A). Finally, the anterior condyles are more prominent on the maximal theoretical shape than on the minimal one (Figs. 3E, 4A).

The distribution along the second axis does not follow variation in body mass (see "Evolutionary Allometry" for details), and specimens with a body mass estimated to more than 1000 kg are located on both sides of the axis, as shown by the circle size (Fig. 3A). However, the distribution along PC 2 highlights a relatively clear separation between pennaraptorans (i.e., the clade closest to birds in our dataset) and other major neotheropod clades along this axis (Fig. 5). Early non-averostran neotheropods from the Late Triassic and Early Jurassic (except one *Coelophysis* specimen out of five) and all ceratosaurians are located on the negative part of the morphospace, whereas all pennaraptorans are located on the positive part of the morphospace (Figs. 3A, 5; Coe). The rest of the dataset (i.e., non-pennaraptoran Tetanurae) is spread across the positive and negative parts but mostly closer to the middle part of the morphospace (Figs. 3A, 5). Among the non-pennaraptoran tetanurans, the earliest representatives of each

https://doi.org/10.1017/pab.2024.6 Published online by Cambridge University Press

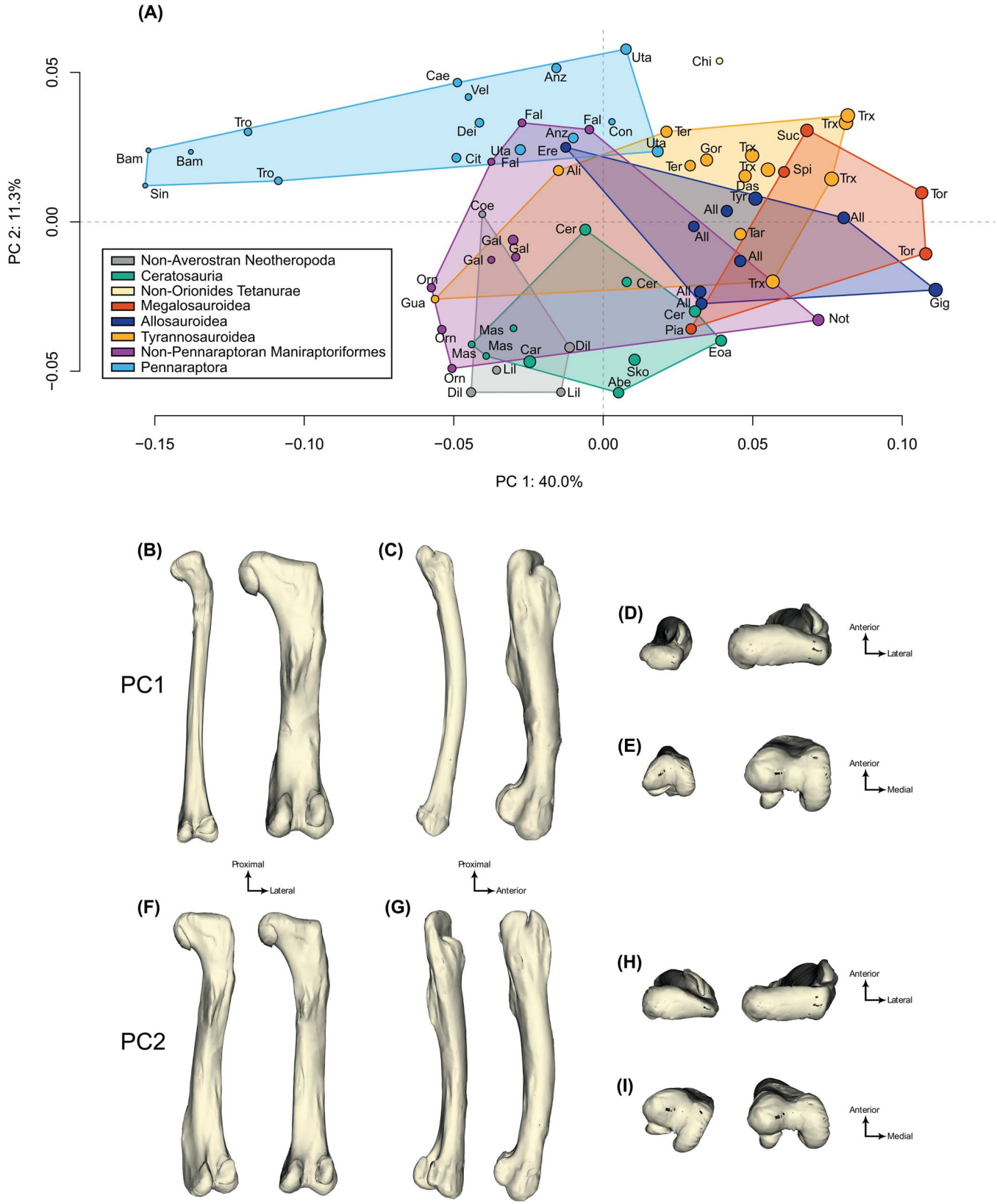

Figure 3. A, The two first axes of the principal component analysis (PCA). Taxonomic abbreviations: see Table 1. Circle diameter is proportional to estimated body mass (see Table 1). Minimal (left) and maximal (right) theoretical shapes for PC 1 (top) and PC 2 (bottom) in posterior (B, F), lateral (C, G), proximal (D, E), and distal (H, I) views.

https://doi.org/10.1017/pab.2024.6 Published online by Cambridge University Press

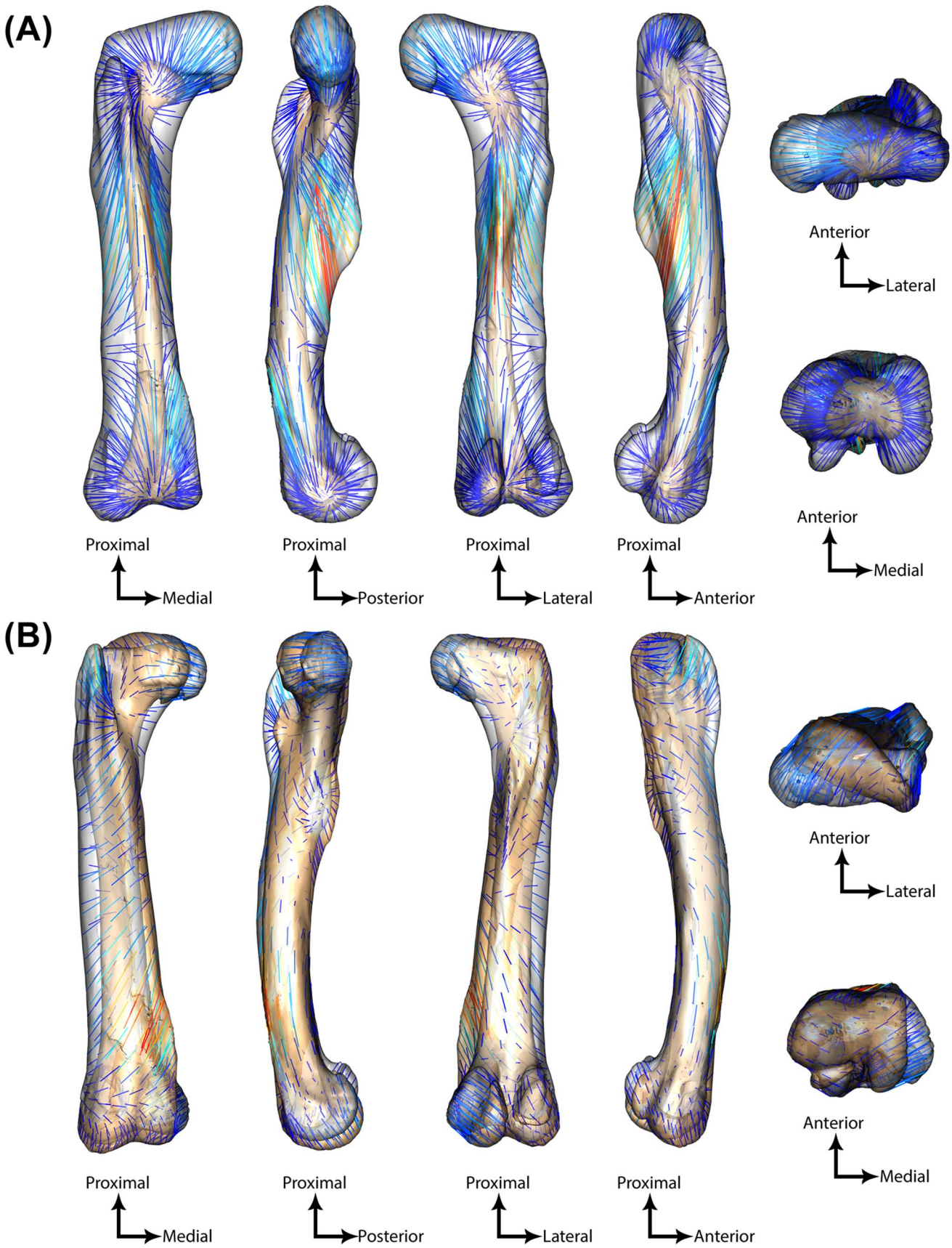

Figure 4. Morphological variation between minimal (colored) and maximal (gray) theoretical shapes along (A) principal component (PC) 1 and (B) PC 2 in anterior, medial, posterior, lateral (from left to right), proximal (top row) and distal (bottom row) views. Intensities of landmark displacements are shown with vector colorations ranging from dark blue (low distance) to red (high distance).

https://doi.org/10.1017/pab.2024.6 Published online by Cambridge University Press

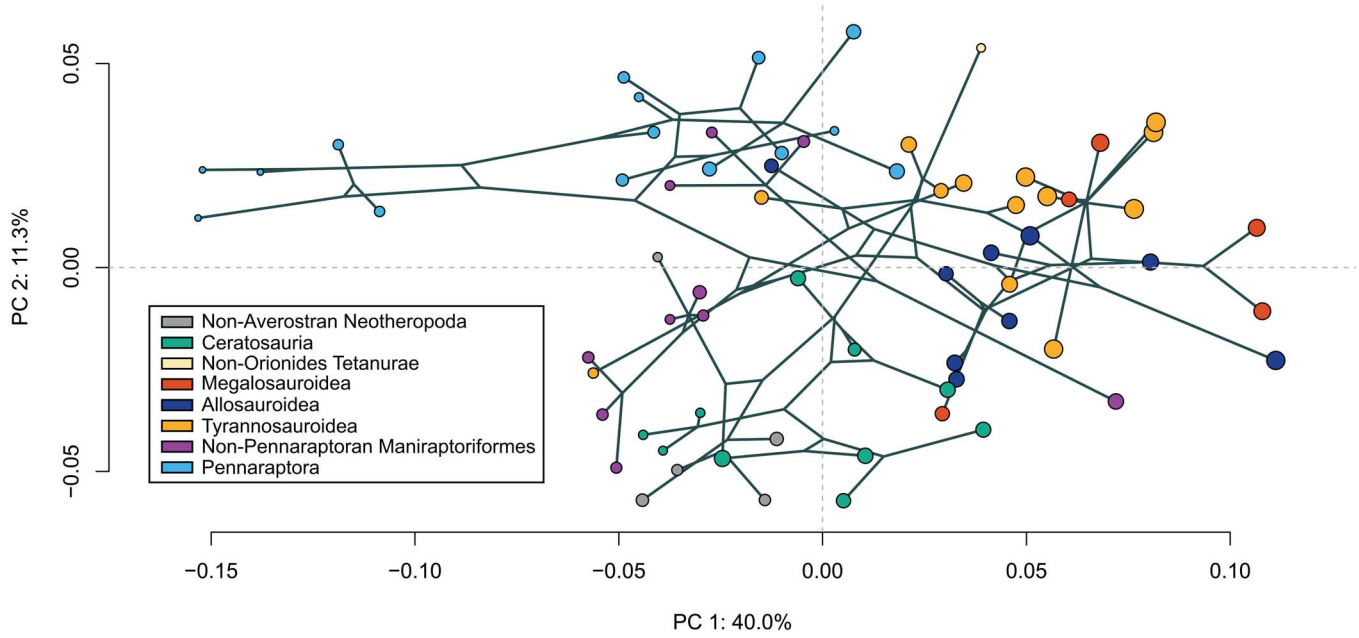

Figure 5. The two first principal component (PC) axes of the phylomorphospace. See Fig. 3A for specimen label.

clade are located closer to the negative side of the axis than the more derived relatives from the same clade, as seen among megalosauroids (i.e., *Piatnitzkysaurus* located more negatively than other megalosauroids or more negatively than *Torvosaurus* and Spinosauridae), tyrannosauroids (i.e., *Guanlong*) and ornithomimosaurians (i.e., ornithomimid indet.; Figs. 3A, 5; Supplementary Fig. S3; Pia, Gua, Ali, Orn, Gal). We made the opposite observations for allosauroids (i.e., *Erectopus*) and therizinosaurs (i.e., *Falcarius*; Fig. 3A; Ere, Fal). Among ceratosaurians, all abelisauroids are closer to the negative side than ceratosaurids (Figs. 3A, 5).

Theoretical shapes along PC 2 highlight that the longest displacement vectors are localized along the proximal part of the mediodistal crest, which is more convex and prominent toward the medial side in the minimal theoretical shape, making it look more sigmoidal (i.e., more curved mediolaterally) than in the maximal theoretical shape (Figs. 3B,F, and 4B). In addition, some of the longest vectors are localized on the proximal area of the lesser trochanter, which is more prominent anteriorly and has a proximal extent equal to that of the greater trochanter on the maximal theoretical shape than on the minimal one (Figs. 3G, 4B). Similarly, the anteroposterior width of the greater trochanter is wider on the maximal shape than on the minimal one, which results in a narrower gap between the greater and lesser trochanter, indicating the fusion of these two tubercles in the taxa on the most positive side of PC 2 (Figs. 3G,H, and 4B). This mostly represents a fusion between the lesser and the greater trochanters toward the pennaraptoran clade (Fig. 5). Finally, there is a greater offset between the epiphyses in the minimal theoretical shape than in the maximal one (Figs. 3H,I, and 4B).

Phylogenetic Signal

Results from the multivariate K statistics highlighted a significant association between femoral morphology and phylogeny when performed on the global variation (K_{mult}) and the two first PC axes individually (K). The phylogenetic signal ratio was clearly below one for the global morphological variation ($K_{mult} = 0.39$, p-value < 0.01), and for the first two PC axes (PC 1: $K = 0.77$, p-value < 0.01; PC 2: $K = 0.49$, p-value < 0.01). These results demonstrated that the morphological variation had a lower phylogenetic signal than predicted by the Brownian motion, indicating that it was also structured within clades (i.e., homoplastic) (Fig. 5).

The phylomorphospace highlights this within-clade variation along PC 1, except for five (out of 15) pennaraptorans (all troodontids and the smallest dromaeosaurid *Bambiraptor*) that are clearly isolated on the negative side from the rest of the specimens (Fig. 5; Bam, Sin, Tro). All other pennaraptorans share similar levels of femoral robusticity with the smallest representatives of the other tetanurans (*Chilesaurus*, *Piatnitzkysaurus*, *Erectopus*, *Guanlong*, *Alioramus*, *Falcarius*, ornithomimid indet.), but also with all non-averostran neotheropods and all ceratosaurians, despite early theropods, ceratosaurs, and maniraptorans being the clades most phylogenetically distant from each other among our dataset (Fig. 5; Chi, Pia, Ere, Gua, Ali, Fal, Orn). The largest representatives of several clades of tetanurans all group together on the most positive side of PC 1, regardless of phylogenetic distinction, as shown by the distance between the two carcharodontosaurids *Tyrannotitan* and *Giganotosaurus* (Fig. 5).

Along PC 2, the earliest representatives of each theropod lineage are located on the opposite side (whether negative or positive) of their later relatives (i.e., *Erectopus* on the most positive part of the allosauroids' morphospace; *Guanlong* on the most negative part of the tyrannosauroids' morphospace; *Piatnitzkysaurus* on the most negative side of the megalosauroids' morphospace; Fig. 5). However, despite the low phylogenetic signal indicated by the K statistics, we observed that the earliest-diverging taxa (non-averostran neotheropods) are mostly grouped on the most negative side of PC 2, whereas later taxa such as non-avian pennaraptorans that are the closest relatives to the avian lineage group on the most positive side of PC 2 (Fig. 5). All other tetanurans group in the middle part of the phylomorphospace (Fig. 5).

https://doi.org/10.1017/pab.2024.6 Published online by Cambridge University Press

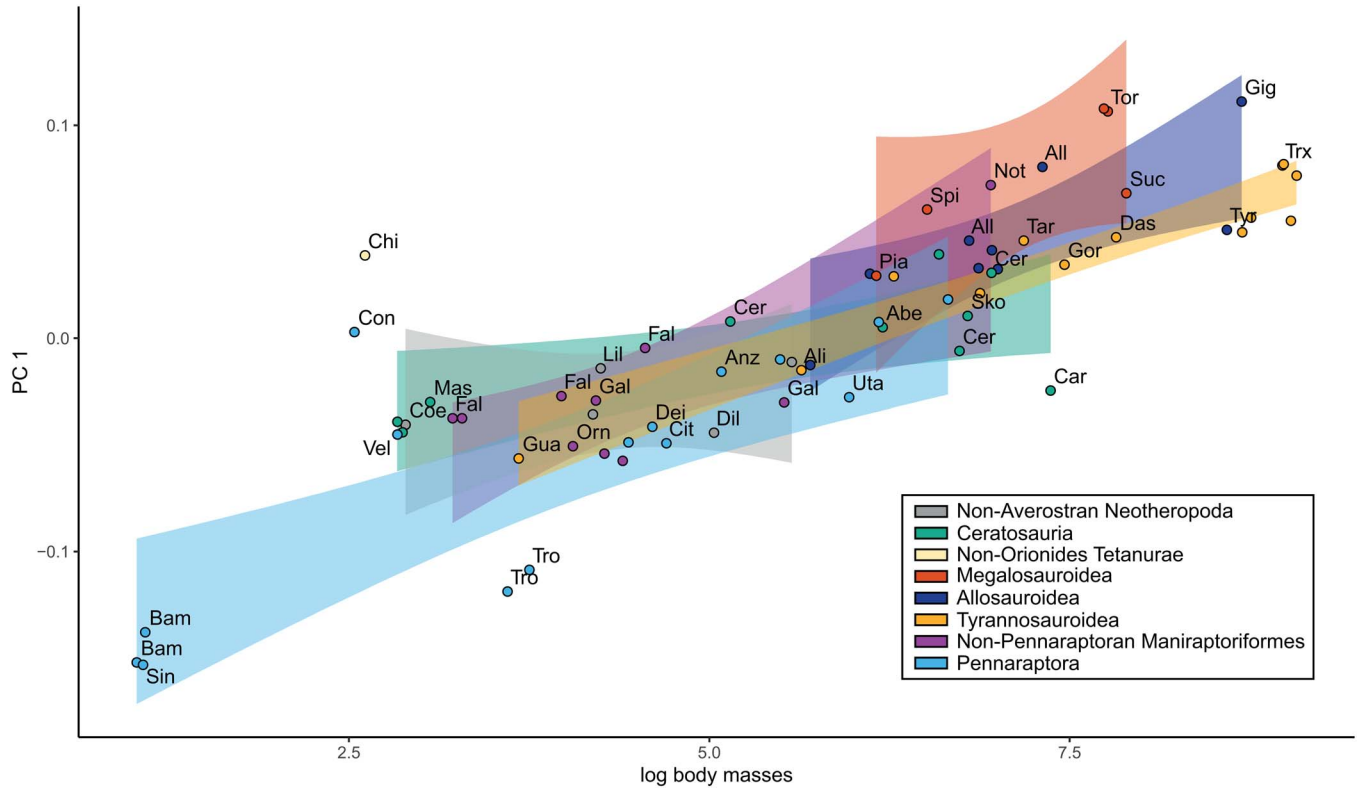

Figure 6. Regression between log-transformed estimated body masses and principal component (PC) 1. Taxonomic abbreviations: see Table 1.

Evolutionary Allometry

We found a strong and positive association when performing Pearson's correlation test between log-transformed centroid size and the distribution along PC 1 (Fig. 6), which mostly represented femoral robusticity ($r^2 = 0.6$, p-value < 0.01), but no significant correlation along PC 2 (p-value > 0.05). We demonstrated an even stronger association when testing for the association between log-transformed estimated body mass (based on MDC) and PC 1 ($r^2 = 0.7$, p-value < 0.01). We obtained similar results when factoring out the phylogenetic resemblance between investigated taxa by computing PGLS at the unidimensional (i.e., isolated PC axis) level on log-transformed centroid size (PC 1: $r^2 = 0.2$, p-value <0.01; PC 2: p-value > 0.05) and log-transformed estimated body mass (PC 1: $r^2 = 0.4$, p-value < 0.01; PC 2: p-value > 0.05). In addition, the PGLS at the multidimensional level (i.e., all PC axes; the complete morphological variation) revealed a significant but low association of the global morphological variation with both log-transformed centroid size ($r^2 = 0.07$, p-value < 0.01) and estimated body mass ($r^2 = 0.09$, p-value < 0.01).

Discussion

Convergent Specialization to Gigantism in Theropods and Other Archosauriforms Relative to the Evolution of Bipedalism

Femoral Specializations to Gigantism in Theropods . A positive relationship between femoral robusticity (i.e., increase of width relative to length) and body mass is well known to occur among quadrupedal mammals and archosaurs (Gregory 1912; Biewener 1983, 1989; Carrano 1998, 2001; Christiansen 1999; Campione and Evans 2012; McPhee et al. 2018; Mallet et al. 2019; Etienne et al. 2021, Pintore et al. 2022a). Furthermore, the increase of femoral robusticity in mammals is often coupled with enlarged muscle insertions located closer to the middle of the shaft, which enables application of greater moments around the hip joint of heavy animals (Hildebrand 1974; Polly 2007; Mallet et al. 2019). Accordingly, the placement of the fourth trochanter (i.e., attachment site for muscles between the femur and the tail) correlated similarly with body mass among non-avian dinosaurs and other archosauriforms, regardless of their locomotor habit (Coombs 1978; Parrish 1986; Carrano 1999; Pintore et al. 2022b). In addition, the integration of both femoral robusticity and displacement of the fourth trochanter proved to be a reliable indicator of a more cursorial or graviportal morphology in bipedal saurischians (i.e., non-sauropod sauropodomorphs and theropods; Coombs 1978; Christiansen 1998; Carrano 1999; Lefebvre et al. 2022; Pintore et al. 2022a). Therefore, this well-established link between femoral robusticity, fourth trochanter displacement, and increase of body mass gives a broader comparative context for studying the evolution of gigantism across various taxa of obligate bipedal dinosaurs.

We highlighted that the same femoral specialization to gigantism occurred convergently within lineages of theropods, as shown by the significant K statistics below one and the positive allometric relationship between femoral robusticity and the increase of body mass (Figs. 3, 4A, 5, 6). Furthermore, we demonstrated that this convergent femoral robusticity evolved different degrees of specializations depending on the maximum body mass within each theropod lineage. Indeed, the same degree of femoral robusticity and fourth trochanter displacement was shared between several theropods with an estimated body mass of approximately 500 kg despite being distantly related within

https://doi.org/10.1017/pab.2024.6 Published online by Cambridge University Press

the theropod clade, such as the largest dromaeosaurid *Utahraptor*, the ceratosaurids *Ceratosaurus nasicornis* and *Skorpiovenator*, the early neotheropod *Dilophosaurus*, and the relatively small tyrannosaurid *Alioramus* (Table 1; Figs. 1, 3, 4A, 5, 6; Uta, Dil, Cer, Sko, Ali). Moreover, the level of femoral robusticity was globally lower in pennaraptorans and ceratosaurids (Figs. 3A, 5, 6). Therefore, the convergent increase of body mass led to similar morphological specializations in the femora of several theropod lineages, whether it led to gigantism (e.g., Ceratosauridae, Megalosauridae, Tyrannosauridae, Allosauridae, non-pennaraptoran maniraptoriforms) or not (pennaraptorans) and regardless of their phylogenetic relationships (Fig. 6). Further, theropods evolved various growth strategies that were previously demonstrated to link with the evolution of gigantism and miniaturizations in theropods (Padian et al. 2001). For example, prolonged growth appears to have been favored by some carcharodontosaurids, whereas accelerated growth was conversely noted in other allosauroids as well as in some tyrannosauroids (Cullen et al. 2020; Canale et al. 2022; D'Emic et al. 2023). Hence, femoral shape specializations to different body masses evolved convergently through different developmental strategies among theropods.

Femoral Specializations to Increasing Body Mass in Earlier Archosaurs. Early archosaur femora evolved similar femoral specializations to body mass increase regardless of their locomotor habits, as shown by large bipedal dinosaurs and quadrupedal pseudosuchians similarly evolving mediolaterally enlarged epiphyses and a more distally located fourth trochanter, much as in later theropods (Pintore et al. 2022a; Figs. 3B,C, and 4A). Moreover, there appears to be a decoupling in fourth trochanter morphology that was more asymmetric in bipedal early archosauriforms than in quadrupeds and more rounded in the most robust femora than in the most gracile ones (Pintore et al. 2022b). However, we did not highlight any variation of symmetry in the fourth trochanter of theropods, which were exclusively bipedal. Conversely, the fourth trochanter was prominent and rounded in larger theropods and flatter in the smaller ones (Figs. 3C, 4A). Even if the fourth trochanter evolved a similar prominence with increasing body mass in both bipedal non-sauropod sauropodomorphs and theropods, theropods did not reach the enormous body masses estimated for sauropods; hence, they never reduced their fourth trochanter to the rather flat morphology seen in sauropods (Lefebvre et al. 2022). This difference could indicate either that (1) beyond a certain body mass (i.e., greater than the heaviest theropods), fourth trochanter specializations to increasing body mass evolved from distal migration along the shaft to a more flat morphology in large secondary quadrupedal sauropodomorphs, as the fourth trochanter was already located close to the middle of the diaphysis in earlier bipedal sauropodomorphs, at least in *Mussaurus* and *Plateosaurus* compared with smaller, earlier-diverging taxa such as *Eoraptor* and *Anchisaurus* (Sereno et al. 2012; Pintore et al. 2022b), and was morphofunctionally constrained from shifting more distally; or (2) a common evolutionary pattern existed between the two clades of saurischians, which diverged after a certain amount of time and/or differences in traits.

However, there were a few differences between femoral specializations to body mass observed between early archosauriforms and theropods. The medial border of the femoral head was proximo-dorsally deflected (i.e., "upturned") among the largest theropods, as seen in the large carcharodontosaurid *Giganotosaurus*, and ventrodistally deflected (i.e. "downturned") among the smallest ones (Figs. 3A,B, and 4A; Gig), whereas it did not vary across early archosauriforms (Pintore et al. 2022b). An upturned femoral head was discussed as an unambiguous synapomorphy of Carcharodontosauridae, which includes many giants (Harris 1998; Brusatte and Sereno 2008; D'Emic et al. 2012; Canale et al. 2015, 2022) but also some smaller, earlier relatives such as *Concavenator* and *Neovenator* (the earliest carcharodontosaurids; Hocknull et al. 2009; Cuesta et al. 2018). This feature was also present in *Australovenator* (the sister taxa of all carcharodontosaurids) but not in smaller, earlier relatives from other tetanuran clades. Harris (1998) noted that early non-averostran theropods and ceratosaurids had a downturned femoral head, whereas abelisaurids and non-carcharodontosaurid tetanurans had a rather horizontal femoral head. However, we observed that the femoral head of all early non-averostran neotheropods and ceratosaurians appeared relatively similar to the rather horizontal femoral head orientation of small-bodied taxa in non-carcharodontosaurid tetanurans (e.g., ornithomimids, therizinosaurids, and dromaeosaurids) instead of downturned (Figs. 3A,B, 4A, 5, and 6). We explain these observations contrasting with those of Harris (1998) by the inclusion of "miniaturized" theropods (i.e., less than 20 kg) in our dataset. Some of these taxa had even more downturned femoral heads than those of early non-averostran neotheropods and ceratosaurians (Table 1; Figs. 3A,B, 4A, 5, and 6). In addition, according to our analysis, large-bodied taxa (<1000 kg) within Allosauridae, Tyrannosauroidea, Megalosauroidea, and Therizinosauridae had an upturned femoral head similar to the condition described in carcharodontosaurids (Figs. 3A,B, 4A, 5, and 6). Bates et al. (2012) suggested that an upturned femoral head could have evolved as an adaptation to greater body mass in carcharodontosaurids, reducing the amount of stress that might be experienced at the femoral head and shaft by decreasing the bending moment arm of hip joint forces applied to the femoral head. Our results also suggest that this feature could result from a progressive specialization to large body mass that may have appeared convergently in several lineages of giant theropods and not exclusively in carcharodontosaurids and that it should be regarded as a continuum rather than a discrete character. Furthermore, the ancestral presence of an upturned femoral head in the carcharodontosaurid lineage but not in smaller, earlier relatives from other tetanuran clades suggests that the original morphology of these animals could have facilitated the evolution of gigantism within this clade, shedding light on why carcharodontosaurids evolved such large body size.

Another difference in the femoral specializations between theropods and early archosauriforms was the enlargement and proximal shift of the mediodistal crest (also termed "medial epicondyle" [Carrano and Sampson 2008] and "craniomedial crest" [Hutchinson 2001]; Figs. 3A,C, and 4A). A well-developed mediodistal crest is a feature exclusive to neotheropods and most likely acted as part of the origin of the femorotibialis musculature (Hutchinson 2001; Carrano and Hutchinson 2002). However, a well-developed crest can be characterized by different morphotypes, with a morphology varying from a smooth, subdued crested to a hypertrophied flange, and with varied extent along the shaft, traits described to distinguish various neotheropod clades (Ezcurra 2006; Carrano and Sampson 2008). First, its enlargement toward the middle of the shaft by 25% at least of the femoral length was described as a carcharodontosaurid synapomorphy (Holtz et al. 2004; Brusatte and Sereno 2008). Second, a hypertrophied flange-like mediodistal crest (i.e., more prominent toward the medial side) is a diagnostic feature of abelisauroids

https://doi.org/10.1017/pab.2024.6 Published online by Cambridge University Press

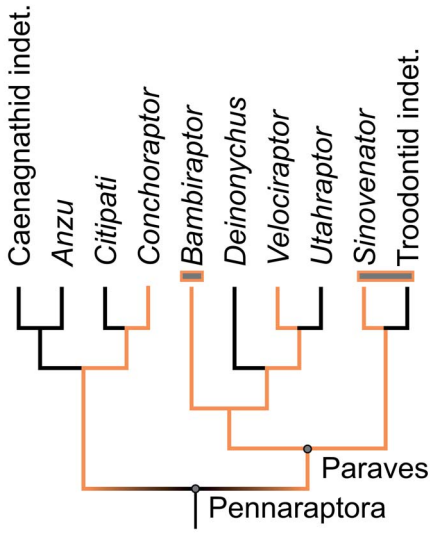

Figure 7. Simplified representation of the evolution of femoral specializations to miniaturization (gray rectangles) across the evolution of miniaturization (orange). Black lineages lack miniaturization. The paravian origin of miniaturization is based on the literature. Our speculation about the possible origin of miniaturization at the pennaraptoran node is based on the "miniaturization" of *Conchoraptor*, which may or may not represent an independent convergent event.

(Carrano et al. 2002; Tykoski and Rowe 2004; Ezcurra 2006; Martinelli et al. 2019), and a long and crest-like crest morphology is present in ceratosauroids (Carrano and Sampson 2008) and other non-abelisauroid neotheropods (Ezcurra 2006), whereas the crest is absent in all coelurosaurs except tyrannosauroids (Novas et al. 2012). Because we demonstrated a decoupling in the mediodistal crest extension between PC 1 (i.e., proximo-distal extension) and PC 2 (i.e., mediolateral extension), this observation is therefore consistent with our results showing that the two abelisauroids *Masiakasaurus* (a small noasaurid) and *Carnotaurus* (a large abelisaurid) clustered together in the PC 1–PC 2 morphospace (Figs. 3A,B, and 4A; Cer, Mas). Accordingly, these specimens should have displayed the greatest development of the mediodistal crest of our dataset (i.e., prominent, hypertrophied, and flange-like), but this was not the case. Indeed, we demonstrated that its proximal extension was similar to those of early neotheropods and other ceratosaurians, and to a lesser degree than in any other neotheropods with a more robust femoral morphology (Figs. 3A,B, and 4A). In addition, and even if its medial extension was greater than that of Tetanurae, it was similar to those of other ceratosaurians and early neotheropods too (Figs. 3A,B, and 4A). This inconsistency indicates that a "well-developed mediodistal crest" should be interpreted as a continuum from either more or less expanded toward the medial side (i.e., prominent) or more or less elongated toward the middle of the shaft (i.e., proximally extended). We demonstrated that the mediodistal crest extended toward the middle of the shaft in large theropods and that it was less prominent in maniraptoran theropods that were the closest relatives to birds (Figs. 3A,B,F, 4A,B, and 5). Moreover, a proximally elongated mediodistal crest in large theropods could indicate biomechanical modifications of femorotibial muscles and/or knee extensor tendons (Hutchinson 2001). Stronger muscular forces along the medial axis of the legs could improve mediolateral stability, vital for the bipedal locomotion of large theropods (Bishop et al. 2017, 2021). Therefore, the morphology of the mediodistal crest was decoupled between the evolution of gigantism (i.e., variation of proximal extension) and the phylogenetic proximity to the bird lineage (i.e., prominence/medial extension), as in the case of the fourth trochanter between small versus large and bipedal versus quadrupedal avemetatarsalians, pseudosuchians, and early archosauriforms (Pintore et al. 2022b).

In conclusion, the femur of several lineages of theropods convergently specialized to the increase of body mass and similarly to other saurischians and archosauriforms, suggesting that a similar femoral Bauplan was replicated during the evolution of archosauriform gigantism while integrating specific innovations for large bipeds.

The Influence of Ecological Habits on Femoral Robusticity

Cursoriality in Carnotaurus. Our results highlighted that not all giant theropods had a robust femoral morphology. Indeed, the largest abelisauroid, *Carnotaurus* (~1500 kg), had a femoral robusticity similar to that of smaller theropods from ~20 to ~500 kg with cursorial morphology, such as *Velociraptor* and *Gallimimus* (Figs. 3A, 6; Car, Vel, Gal). The ceratosaurian with the closest femoral robusticity was the smallest of all abelisauroids, *Masiakasaurus* (~20 kg), while medium-sized abelisauroids such as *Skorpiovenator* and *Eoabelisaurus* (~800 kg) had greater femoral robusticity than *Carnotaurus* (Figs. 3A, 6; Mas, Sko, Eoa). It was previously suggested that *Carnotaurus* had an unusually athletic morphology, on the basis of its tibial length being relatively longer than its femoral length and on the prominent, dorsally inclined transverse processes on the caudal vertebrae; the latter suggests an enlarged caudofemoralis muscle, which attaches on the fourth trochanter at the posterior side of the femur (Bonaparte et al. 1990; Mazzetta et al. 1998; Persons and Currie 2011). Persons and Currie (2011) speculated that the possible heightened athleticism of *Carnotaurus* might have evolved because of the competition they may have encountered with carcharodontosaurids, which lived in the same geographic area and were much larger than any abelisauroid. Whether this hypothesis is valid remains untested, but even if the carcharodontosaurids *Giganotosaurus* and *Tyrannotitan* appeared earlier than the first known occurrence of *Carnotaurus*, we show a definite morphofunctional distinction between those taxa. Indeed, the femoral morphology of carcharodontosaurids was among the most robust (e.g., *Tyrannotitan* and *Giganotosaurus*), contrasting with *Carnotaurus* having the most gracile morphology of all giant theropods (Table 1; Figs. 3A, 6; Car, Gig, Tyr).

Semi-aquatic Lifestyle in Spinosaurus. The femur of the megalosauroid *Spinosaurus* led to a surprisingly small body mass estimation (~600 kg; Table 1) given its extreme estimated body length of approximately 14 m (Sereno et al. 2022) and its high level of femoral robusticity (Figs. 3A, 6). Indeed, *Spinosaurus*'s femoral robusticity was similar to that of the other large spinosaurid genera *Suchomimus* and megalosauroid *Torvosaurus*. Ibrahim et al. (2014) described the *Spinosaurus* femur as short and robust, resulting in an unusually low ratio of hindlimb length to total body length relative to other theropods (27% in *Spinosaurus* vs. 40% in *Suchomimus* and even greater in other theropods). This reduction of the hindlimb length while preserving a high femoral robusticity was suggested as indicating an aquatic lifestyle for *Spinosaurus* and potentially a quadrupedal habit (Ibrahim et al.

https://doi.org/10.1017/pab.2024.6 Published online by Cambridge University Press

2014, 2020; Fabbri et al. 2022). However, this hypothesis was extensively discussed by other authors, who favored a semi-aquatic to terrestrial lifestyle (Amiot et al. 2010; Hone and Holtz 2021; Sereno et al. 2022). Furthermore, this contrast between high femoral robusticity and low estimated body mass might be explained by the MDC-based body mass estimation method we used not being appropriate for a theropod with ecological and locomotor habits different from fully terrestrial bipedality. Another explanation could be that FSAC KK11888 was actually estimated to be only 76% of the maximum known body length for *Spinosaurus* (Sereno et al. 2022). Ibrahim et al. (2014) demonstrated that this individual was not a juvenile by estimating its age to be around 17 years old through histological analysis, and suggested that FSAC KK11888 was most likely a subadult, as Sereno et al. (2022) also did. An absence of variation of femoral robusticity along ontogeny was also observed among juvenile and adult semi-aquatic Nile crocodiles (Pintore et al. 2022b). Indeed, the femoral robusticity of these taxa was as high as in the Late Triassic quadrupedal semi-aquatic phytosaurs, quadrupedal pseudosuchians such as armored aetosaurs (e.g., *Typothorax* and *Paratypothorax*), and large bipedal sauropodomorph dinosaurs (e.g., *Plateosaurus* and *Mussaurus*; Pintore et al. 2022b). In light of the presumed at least semi-aquatic lifestyle of *Spinosaurus*, the high robusticity of its femur relative to its estimated age, body mass, and length appears consistent with the condition observed across different ontogenetic stages of semi-aquatic quadrupedal archosaurs. This observation reinforces the hypothesis that both the evolution of some degree of amphibious/semi-aquatic lifestyle and gigantism convergently led to a high femoral robusticity in archosauriforms, regardless of locomotor habit. Although a similar convergent phenomenon was demonstrated in the internal bone structure of both semi-aquatic and graviportal amniotes (Houssaye et al. 2016, 2021), this parallel has not been highlighted in the external morphology of their bones.

The Evolution of Miniaturization and Its Associated Femoral Specialization

As discussed by Benson et al. (2018), the multiple originations of gigantism represent only one facet of the evolutionary history of dinosaur body mass. Whereas it seems that there was a single allometric trajectory to evolve femoral robusticity along increasing body mass within theropods, it does not seem to be the case with femoral gracility along decreasing body mass (Figs. 3A, 6). Instead, the rather gracile femora were subdivided into two clusters, one containing most of the medium-sized cursorial taxa in our dataset (e.g., *Gallimimus*, *Deinonychus*, *Masiakasaurus*, *Falcarius*; Fig. 3A; Gal, Dei, Mas, Fal), and one containing only "miniaturized" theropods (i.e., with body masses between 1 to 20 kg, lighter than the lightest earlier taxa; e.g., the dromaeosaurid *Bambiraptor* and the troodontid *Sinovenator*; Figs. 3A, 6; Bam, Sin). Whether theropods experienced a sustained size decrease during their evolutionary history (Turner et al. 2007; Lee et al. 2014) or a more punctuated mode of evolution (Carrano 2006; Benson et al. 2018), most studies agree that a drastic reduction in body mass occurred close to the bird lineage of Avialae (Brusatte et al. 2014), specifically around the paravian node (Turner et al. 2007; Benson et al. 2014). This theropod miniaturization was even previously documented as the plesiomorphic condition for all earlier bird relatives, which later facilitated the evolution of key innovations such as powered flight (Sereno 1999; Xu and Norell 2004; Carrano 2006; Turner et al. 2007). We suggest that this accelerated miniaturization close to the bird lineage was associated with certain femoral specializations (i.e., long diaphysis relative to epiphyseal width, proximo-distally reduced fourth trochanter located close to the femoral head, downturned femoral head, mediodistal crest proximo-distally reduced), as represented by the cluster integrating the most gracile femora. Furthermore, this specialization is not observed among small early-diverging non-tetanuran theropods with an estimated body mass less than ~20 kg, because they are not included in the cluster (e.g., the Late Triassic *Coelophysis* and *Masiakasaurus*, the smallest ceratosaurian from the Late Cretaceous; Figs. 3A, 5; Coe, Mas). Thus, this specialization was not linked only to small body size but rather seemed restricted only to a few paravian clades, consistent with the main miniaturization event on line to birds (Figs. 3A, 6, 7).

However, some "miniaturized" paravians and non-paravian pennaraptorans had an unusually high femoral robusticity relatively to their estimated body mass (e.g., the smallest oviraptorid *Conchoraptor* and the dromaeosaurid *Velociraptor*; Figs. 3A, 6; Con, Vel) and did not plot along with other "miniaturized" theropods such as *Bambiraptor* and *Sinovenator* (Figs. 3A, 6; Bam, Sin). For example, *Conchoraptor* was the only "miniaturized" non-paravian pennaraptoran from our sample, as we estimated its body mass to be around 13 kg (Table 1; Figs. 3A, 7), which was consistent with other studies (Kundrát 2007; Balanoff et al. 2013, 2014). Therefore, the timing of the main miniaturization event on line to crown birds could have occurred earlier than the paravian node, at the pennaraptoran node (as displayed in Fig. 7), although the "miniaturization" of *Conchoraptor* could also be an independent convergent occurrence. Nevertheless, the femur of *Conchoraptor* did not specialize to "miniaturization" as in other dromaeosaurids and troodontosaurids from our dataset. Hence, specialization to miniaturization did not evolve in small oviraptorosaurids, whereas it did in the smallest dromaeosaurids and troodontids (Fig. 7). Conversely, some troodontids had an unusually low femoral robusticity given their estimated body mass (Table 1; Fig. 6; Tro), which may be related to the fairly cursorial morphology, such as relatively elongated legs and metatarsals for their body size observed for this clade (Holtz 1994). This observation further highlights that, while there was a main miniaturization event that was ancestral for several pennaraptoran clades, its associated femoral specialization occurred only later within paravians and may have been preserved during subsequent distinct events of body mass increase. This could indicate either that: (1) femoral specialization to miniaturization evolved once around the paravian node and was preserved along the later increase of body mass in troodontids (*Sinovenator* ~ 3 kg, Troodontidae indet. ~ 40 kg) but not in the later increase of body mass in dromaeosaurids (*Velociraptor* ~ 20 kg; *Deinonychus* ~ 100 kg; *Utahraptor* ~ 550 kg; Fig. 7); or (2) femoral specialization to miniaturization convergently evolved only among some paravians (*Bambiraptor* and troodontids) from a rather medium-sized cursorial morphology (Fig. 7). However, these hypotheses are complicated by uncertainties in dromaeosaurid phylogenetic relationships (e.g., Turner et al. 2012). We caution that these evolutionary scenarios could vary depending on the phylogenetic positions of *Bambiraptor* and *Utahraptor* (the smallest and largest dromaeosaurids within our sample), which could have diverged earlier within dromaeosaurids than in our composite phylogeny (Fig. 1). Nevertheless, our results improve

https://doi.org/10.1017/pab.2024.6 Published online by Cambridge University Press

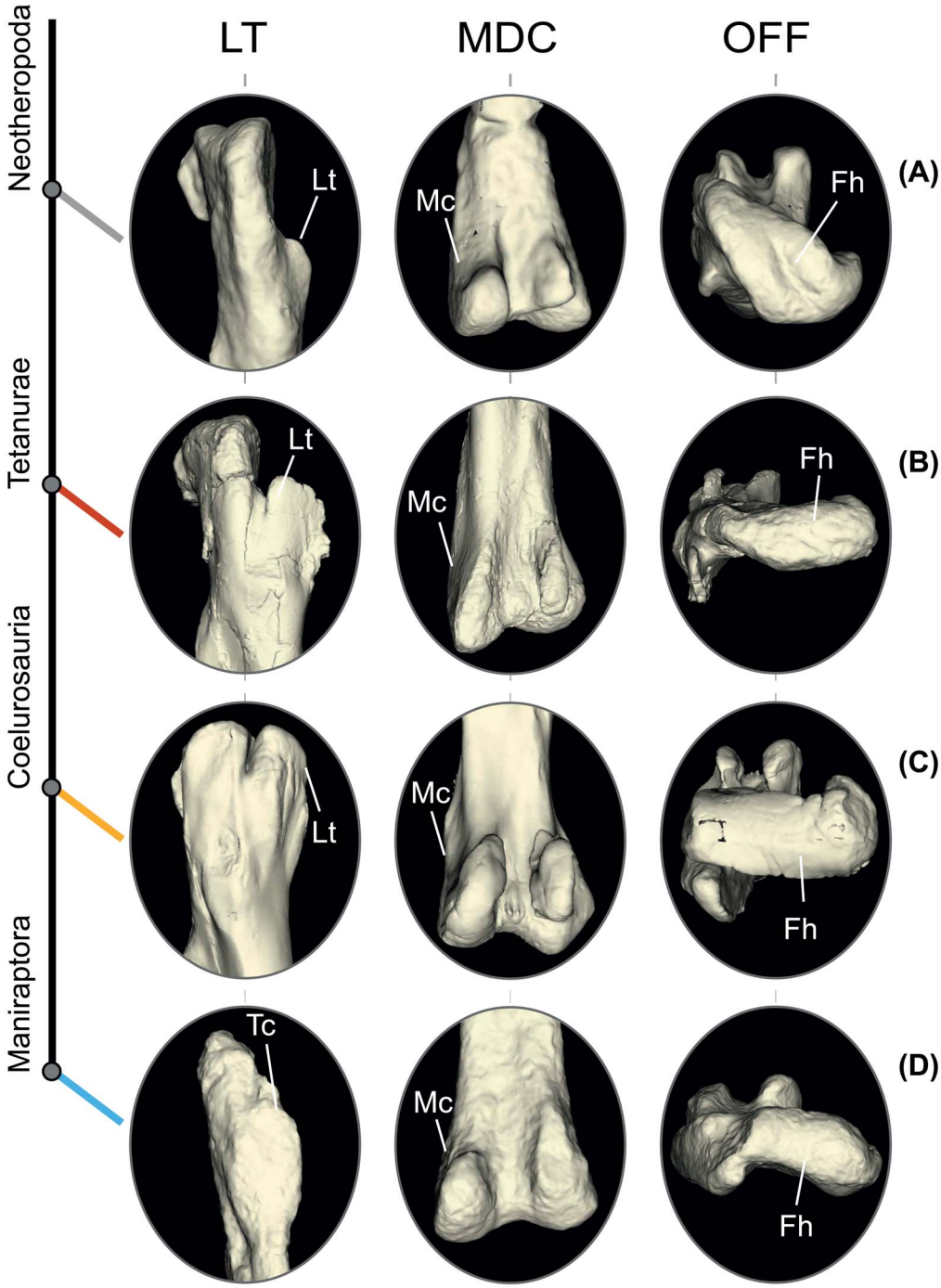

Figure 8. Mosaic evolution of the "avian"-like femoral features (Fh, femoral head; Lt, lesser trochanter; Mc, mediodistal crest; Tc, lesser and greater trochanters fused in trochanteric crest) in different theropod lineages, illustrated with the femur of (A) *Lilienstern*us (specimen 2), (B) *Suchomimus*, (C) *Tyrannosaurus* (FMNH PR 2081), and (D) *Deinonychus* in lateral (LT), posterior (MDC), and proximal (OFF) views. Colors: gray, non-averostran neotheropods; red, megalosauroids; yellow, tyrannosauroids; light blue, pennaraptorans. Abbreviations: LT, proximal extension of the lesser trochanter; MDC, more convex or concave shape of the mediodistal crest; OFF, more or less medial offset of the femoral head relative to the distal epiphysis.

understanding of how miniaturization evolved close to the bird lineage. The femoral specialization to miniaturization evolved only from the paravian node and onward, potentially convergently between some dromaeosaurids and troodontids, but was not shared with non-paravian theropods of similar body mass or with paravians closely related to the relatively large dromaeosaurid *Utahraptor* (Figs. 3A, 6, 7). This raises the question of whether the origins of a rather "avian" femoral morphology (i.e., fused greater and lesser trochanters, no epiphyseal offset, reduced and concave mediodistal crest) across the pennaraptoran node were independent from the femoral specialization to miniaturization.

https://doi.org/10.1017/pab.2024.6 Published online by Cambridge University Press

Was the Evolution of the Avian Femoral Morphology Independent from the Specialization to Miniaturization?

Taxa that were the most distantly related to the avian lineage had the femora with the most sigmoidal shape, with a slight medial offset of the femoral head in relation to the distal epiphysis, a convex and prominent mediodistal crest, and well-separated greater and lesser trochanters. Moreover, the lesser trochanter had a lower proximal extension than the greater trochanter (Figs. 3A, F–I, 4B, and 5). Conversely, taxa that were closer to the bird lineage had straighter femora with little to no epiphyseal offset, a reduced and concave mediodistal crest, along with extension of the lesser trochanter to the same proximal level as that of the greater trochanter (Figs. 3A,F–I, 4B, and 5). These latter morphological variations mostly occurred convergently, but to a greater extent in clades that were phylogenetically closer to the bird lineage (Fig. 5). Therefore, we interpret the combination of these femoral features to represent a more "avian"-like morphology.

Lesser Trochanter. The lesser trochanter in dinosaurs is thought to have been the attachment site for the iliotrochantericus caudalis (ITC) muscle (Hutchinson 2001), which was key in the transition from hip-based to knee-based locomotion toward crown birds and is thus characteristic of avian locomotion (Hutchinson and Gatesy 2000; Allen et al. 2021). The proximal extension of the lesser trochanter, and its subsequent fusion with the greater trochanter, gradually evolved from earlier theropods toward birds, perhaps to accommodate an anteroproximal shift of the ITC insertion (Carrano 2000; Hutchinson 2001). This shift may have increased the capacity of the ITC to cause internal (medial) long-axis rotation of the femur, providing mediolateral forces in order to keep legs close to the sagittal midline and maintain balance during the stance phase in bipedal and erect archosaurs, especially with a more or less knee-based locomotion (Hutchinson and Gatesy 2000). It was previously demonstrated that an actual fusion between greater and lesser trochanters only evolved within maniraptoran theropods, except in therizinosaurs, which preserved a narrow intertrochanteric groove (Chiappe et al. 1997; Hutchinson and Gatesy 2000; Holtz and Osmólska 2004). Yet the proximal extension of the lesser trochanter (i.e., without evolving an actual fusion with the greater trochanter) evolved earlier than Maniraptora in Coelurosauria (Gauthier 1986; Hutchinson 2001). Accordingly, we have highlighted that the greatest level of proximal extension of the lesser trochanter evolved earlier than Maniraptora along the theropod phylogeny in tyrannosaurids (Figs. 3A,C, and 8C). The proximal extension of the lesser trochanter was low in the Late Jurassic early-branching tyrannosaurid *Guanlong* and gradually increased toward the Late Cretaceous giant *Tyrannosaurus* and its close relatives. The ITC is an important component of weight support in single-limb stance (regardless of mechanism; i.e., abduction or long-axis rotation), and changes in its insertion reflect increases in the weight this muscle may have been supporting—either via absolutely larger masses (e.g., as in tyrannosaurids; Figs. 3A,C, and 8C) or via doing a greater fraction of the load-sharing as part of more knee-driven locomotion (Hutchinson and Gatesy 2000; Allen et al. 2021). This suggests that a shift of the ITC insertion correlated with variation in body mass within at least one lineage (e.g., tyrannosauroids) not closely related to the avian lineage (Figs. 3A, 8, Supplementary Fig. S4; Gua, Trx). Therefore, this observation suggests a more complex link between body mass support, limb kinematics, and ITC insertions. However, we did not observe any variation of proximal extension in the earliest-branching neotheropods (non-averostran neotheropods and ceratosaurians) or in non-coelurosaurian tetanurans (megalosauroids and allosauroids; Figs. 3A, 8B). This observation suggests a mosaic evolution of the proximal extension of the lesser trochanter, which independently evolved to a different degree exclusively among clades that were closer to the bird lineage (Fig. 8B).

Epiphyses Offset. While no variation of lesser trochanter extension and mediodistal crest prominence was visible along the megalosauroid lineage, there was a greater epiphyseal offset in the early Lower Jurassic megalosauroid *Piatnitzkysaurus* than in the Late Jurassic megalosaurid *Torvosaurus* and spinosaurids from the Lower Cretaceous, *Spinosaurus* and *Suchomimus*, the latter having the most parallel alignment between the two epiphyses (Fig. 3A,H,I; Pia, Tor, Suc, Spi; Fig. 8, OFF). A lower epiphyseal offset reflects improved protraction/retraction motions of the femur, which is associated with more parasagittal limb posture (Carrano 2000; Hutchinson and Gatesy 2000), commonly associated with the archosaurian erect posture and, more relevant here, the evolution of more knee-based locomotion toward birds (Farlow et al. 2000; Hutchinson and Allen 2009). Yet although a shift in epiphyseal offset evolved within theropods toward crown-group birds (Egawa et al. 2022), it also convergently appeared several times within other dinosaur clades (e.g., Ornithischia and Sauropodomorpha; Carrano 2000; Hutchinson 2001). Therefore, our observations further characterize the convergent nature of femoral epiphyseal offset by demonstrating its occurrence along non-coelurosaurian lineages, which diverged earlier than the avian lineage within Theropoda.

Mediodistal Crest. Finally, the variation of the mediodistal crest prominence had a wide phylogenetic span, with no apparent allometric relationship with body mass. Indeed, only the clades most distantly related to the bird lineage had a prominent convex mediodistal crest (Figs. 3A,F, 4B, and 8A). Among tetanurans, non-pennaraptorans had a somewhat intermediate "smooth" condition, with little to no medial extension along each lineage (megalosauroids, allosauroids, tyrannosauroids, therizinosauroids, ornithomimosaurids), except for some *Allosaurus* specimens having a surprisingly prominent crest. In contrast, all pennaraptorans had a clearly concave mediodistal crest (Fig. 8D). Therefore, modification from a rather convex to concave mediodistal crest may reflect a functional shift from earlier theropods to birds, which is consistent with its variation along the phylogeny of theropods of our dataset. However, and because we demonstrated that two (out of three) "avian" femoral features (i.e., lesser trochanter extension and epiphyseal offset) evolved convergently within Theropoda, we suspect that the phylogenetic signal of the mediodistal crest variation was overlooked by the K statistics ($K < 1$). Nevertheless, we discussed earlier that the proximal extension, instead of the prominence, of the mediodistal crest was associated with an increase of body mass. Thus, our result highlighted a decoupling between variations of body mass and the evolution of avian/knee-based locomotor mechanisms in the mediodistal crest morphology (Figs. 3, 4, 8). This may suggest a mosaic evolution in femorotibialis muscle anatomy along with body mass and locomotor variations.

Mosaic Evolution of a More "Avian" Femoral Morphology. Carrano (2000) stated that dinosaurs had three fundamental

https://doi.org/10.1017/pab.2024.6 Published online by Cambridge University Press

transformations during the evolution of parasagittal hindlimb function: (1) a reorientation of the femoral head toward a fully medial direction, (2) the proximal extension of the lesser trochanter, and (3) changes of the ilium, the last of which is not directly relevant to our study. Our results highlighted that the two major femoral transformations were independent from variations of body mass (Figs. 3A,G–I, and 4B; Supplementary Fig. S4). Similar changes (i.e., lesser trochanter extension and epiphyseal offset) evolved convergently between three major clades of dinosaurs (theropods, sauropodomorphs, and ornithischians; Coombs 1978; Gauthier 1986; Novas 1996; Carrano 2000; Hutchinson 2001), and we demonstrated additional convergent evolutions of the same features within neotheropods as well (Fig. 8). We interpret this as further emphasizing that transformations experienced by Mesozoic theropods along the lineage to birds did not follow a gradual increase from the taxa most distantly related to the most closely related to birds, as noted in Carrano (2000; e.g., megalosauroids from deeply nested lineages had a more similar femoral "avian" morphology to pennaraptorans and tyrannosauroids than other theropods more closely related to birds). Instead, we suggest that repeated iterations of femoral transformations within several lineages may have led to more derived bipedal functions (i.e., more "avian" style of locomotion) in dinosaurs, ultimately shifting from more hip- to more knee-driven locomotor habits in paravians. Consequently, the "avian" femoral morphology may have evolved in a mosaic fashion, which may have started to evolve deep within the evolutionary history of dinosaurs and followed, just like miniaturization, either a long sustained trend or a somewhat stepwise pattern, but without any clear, binary distinction between "non-avian" and "avian" femoral morphology (Hutchinson and Allen 2009; Brusatte et al. 2014; Benson et al. 2018).

Specialization to Miniaturization Evolved Only in the Most "Avian" Femoral Morphology. Although it is evident that some of the most "avian" femoral morphologies (i.e., straight femur with no epiphyseal offset, reduced and concave mediodistal crest, lesser trochanter proximally extending to the level of greater trochanter) appeared only in "miniaturized" taxa and close relatives, we demonstrated no apparent link with variation in body mass (Figs. 3A, 5–7). However, while the first occurrence of miniaturization may have evolved in maniraptorans, we demonstrated that the actual femoral specializations to miniaturization (i.e., long diaphysis relative to epiphyseal width, proximo-distally reduced fourth trochanter located close to the femoral head, downturned femoral head, mediodistal crest proximo-distally reduced) appeared only in some paravians, which already integrated fundamental modifications toward a rather "avian" femoral morphology (Figs. 3, 5, 7, 8; Supplementary Fig. S4; i.e., a concave mediodistal crest appeared only in pennaraptorans; a complete fusion between greater and lesser trochanter evolved in maniraptorans; a full medial offset of the femoral head first evolved in megalosauroids). Thus, only theropods with the most "avian"-like femoral morphology evolved a highly derived specialization to miniaturization (Figs. 3A, 7, 8). This pattern is consistent with findings from Benson et al. (2014) that maintaining small body size was key to evolving essential avian features. Furthermore, an increase of body mass evolved within paravians, as seen with *Utahraptor* having one of the most "avian" femoral morphologies of the dataset while having an estimated body mass of ~550 kg. This striking example highlights that theropods closely related to birds could evolve "avian"-like femoral features while independently evolving the same femoral specializations to gigantism as any other earlier giant relatives, but without reverting to a plesiomorphic condition of overall femoral morphology. Therefore, even if a more "avian" femoral morphology is a specialization to miniaturization, it did not limit later evolutionary increases of body mass. Further, large body mass also evolved in Cenozoic crown-group birds to an estimated maximum of 500 to 700 kg (e.g., *Dromornis stirtoni*; see Chinsamy et al. 2023). Although much larger than the inferred mass of the ancestral bird (Benson et al. 2014), their estimated maximum body mass is still well below the upper limit reached among non-avian theropods. This has led to different hypotheses that body mass increases in crown birds were constrained by various factors, such as the resistance of their eggshell presumably limiting the body mass of the incubating individual (Deeming and Birchard 2009). Another possible constraint would have been the more anteriorly located center of mass associated with a more "avian" knee-based locomotion, which would have constrained the femoral morphology to withstand specific bending stresses, hence limiting the evolution of specialization to extreme body mass increases, which may have been more possible in the typically more vertically oriented femora of many non-avian theropods (Gatesy 1991; Chan 2017). Indeed, a more knee-based locomotion (i.e., more flexed hindlimb, more horizontal femur) is associated with increased torsional loads on the femur and relies less on femoral abductors than hip-driven bipedal locomotion does (Carrano 2000; Hutchinson and Gatesy 2000; Hutchinson and Allen 2009), hence differing from the condition in some earlier-diverging theropods. We suggest that this relationship between specialization of body mass increase and a somewhat "avian" femoral morphology may have been facilitated by the morphological decoupling of mediodistal crest evolution. Further investigations of femoral morphology and how it related to biomechanical constraints across miniaturized to giant Mesozoic and Cenozoic paravians could yield new evidence on how repeated variations of body mass in theropods could have evolved along the line to birds, independent of or related to the evolution of the avian Bauplan.

Conclusion

Our study demonstrates that the femoral morphology of obligately bipedal theropods consistently evolved similar specializations to gigantism regardless of their phylogenetic affinities, maximal body mass, and (inferred) degree of hip-/knee-driven locomotor mechanism. Femoral robusticity increased convergently between several theropod lineages through a consistent shift of the fourth trochanter toward the middle of the shaft, a mediolateral enlargement of the epiphyses, a proximodorsal reorientation of the medial side of the femoral head, and a proximal enlargement of the mediodistal crest. Some of these features, such as the distal shift of the fourth trochanter and the enlargement of the epiphyses, are common specializations to gigantism known in quadrupedal dinosaurs and other vertebrates. However, variations relative to the proximodorsal orientation of the femoral head and the proximal extension of the mediodistal crest may be exclusive to gigantism in theropod dinosaurs. These features could reflect the functional constraints experienced by femora of giant bipeds with increasingly vertically oriented hindlimbs. In contrast, some paravians demonstrated an extreme degree of femoral gracility, which we interpreted as a specialization to miniaturization. This specialization was not common to all small, potentially "miniaturized" (less than ~20 kg), derived theropods (i.e., not all pennaraptorans). Only "miniaturized"

https://doi.org/10.1017/pab.2024.6 Published online by Cambridge University Press

pennaraptorans that acquired at least three key femoral "avian" features (i.e., fusion between the greater and lesser trochanters, fully medial offset of the femoral head, concave mediodistal crest) displayed a strong specialization to miniaturization. Accordingly, a rather "avian" femur did not prevent the later evolution of specialization to gigantism in *Utahraptor*, which is large relative to other dromaeosaurids (~550 kg). Furthermore, we hypothesized a decoupling between the evolution of gigantism and more knee-based locomotion in the mediodistal crest morphology. While the crest's proximal extension was linked to an increase in body mass across several lineages, its shape varied from more convex and prominent in the earliest-branching theropods to concave and reduced in the closest relatives to the bird lineage. Therefore, the evolution of a more avian femoral morphology was independent from the repeated occurrence of gigantism, but the two were not mutually exclusive. A thorough investigation of the convergent femoral specializations to large body mass within theropods, bipedal early sauropodomorphs, and more or less quadrupedal/bipedal habits in ornithischians could yield new insights into how dinosaurian hindlimbs accommodated the evolution of gigantism without gradually evolving more knee-driven "avian" locomotion.

Acknowledgments. The data acquisition step of this study was largely impeded by the COVID-19 pandemic because of traveling restrictions. Creating a dataset of this quality would have never been possible without the help of many people around the world. We are indebted to them for providing high-quality data (3D models and photographs) of theropod femora, which were essential to our study: J. Canale and D. Palombi (MMCH); D. Pol (MPEF); T. Szczygielski and J. Słowiak (ZPAL); C. Kammerer, A. Canoville and L. Zanno (NCSM); C. Levitt-Bussian, R. B. Irmis, C. Webb and P. Policelli (UMNH); J. B. Scannella (MOR); B. Strilisky and D. M. Henderson (TMP); A. A. Farke (Raymond M. Alf Museum, USA); X. Yao (Yunnan University, China); J. Molnar (New York Institute of Technology, USA); C. Yu (AMNH); H. Mallison (Palaeo 3D, Germany); P. J. Makovicky (University of Minnesota, USA); P. Sereno; S. Baumgart (FMNH); D. Vidal (Universidad Autónoma de Madrid, Spain); N. Myhrvold (Intellectual Ventures, USA); T. Souter (Independent designer, France); and X. Xing (IVPP). We also warmly thank C. Colin-Fromont, V. Pernègre, J. Barbier, and R. Allain (MNHN), J.-F Tournepiche and D. Augier (Musée d'Angoulême, France). We thank R. Allain, R. Cornette, E. Guilbert, C. Bader, C. Etienne, and R. Lefebvre (MNHN), S. C. R. Maidment (Natural History Museum, UK), S. E. Pierce (MCZ), S. L. Brusatte (University of Edinburgh, UK), and C. Mallet (Institut Royal des Sciences Naturelles, Belgium) for helpful discussions and recommendations about analyses and interpretation of data. Finally, we thank three reviewers (two anonymous and C. T. Griffin) for their constructive feedback and stimulating discussions, which improved the quality of our article.

Funding. This research was supported by the European Research Council under Horizon 2020 Starting Grant GRAVIBONE (715300 to A.H.) and Advanced Grant DAWNDINOS (695517 to J.R.H.); an Australian Government Research Training Program Scholarship (to P.J.B.), the Paleontological Society (Robert J. Stanton and James R. Dodd Award, to P.J.B.), and the International Society of Biomechanics (Matching Dissertation Grant, to P.J.B.).

Competing interests. The authors declare no competing interest.

Data Availability Statement. Data available from the Dryad Digital Repository https://doi.org/10.5061/dryad.tx95x6b52.

Literature Cited

Adams, D. C. 2014a. A generalized K statistic for estimating phylogenetic signal from shape and other high-dimensional multivariate data. *Systematic Biology* **63**:685–697.

Adams, D. C. 2014b. A method for assessing phylogenetic least squares models for shape and other high-dimensional multivariate data. *Evolution* **68**:2675–2688.

Adams, D. C., and E. Otárola-Castillo. 2013. geomorph: an r package for the collection and analysis of geometric morphometric shape data. *Methods in Ecology and Evolution* **4**:393–399.

Adler, D., and D. Murdoch. 2020. rgl: 3d visualization device system (OpenGL), R package version 0.100.54. https://CRAN.R-project.org/package=rgl.

Allain, R. 2005. The enigmatic theropod dinosaur *Erectopus superbus* (Sauvage 1882) from the Lower Albian of Louppy-le-Château (Meuse, France). Pp. 72–86 *in* Kenneth Carpenter, ed. *The carnivorous dinosaurs*. Indiana University Press, Bloomington.

Allain, R., R. Vullo, J. Le Lœuff, and J. F. Tournepiche. 2014. European ornithomimosaurs (Dinosauria, Theropoda): an undetected record. *Geologica Acta* **12**(2).

Allen, V. R., B. M. Kilbourne, and J. R. Hutchinson. 2021. The evolution of pelvic limb muscle moment arms in bird-line archosaurs. *Science Advances* **7**:eabe2778.

Amiot, R., E. Buffetaut, C. Lécuyer, X. Wang, L. Boudad, Z. Ding, F. Fourel, *et al.* 2010. Oxygen isotope evidence for semi-aquatic habits among spinosaurid theropods. *Geology* **38**:139–142.

Bakker, R. T., and P. M. Galton. 1974. Dinosaur monophyly and a new class of vertebrates. *Nature* **248**:168–172.

Balanoff, A. M., G. S. Bever, T. B. Rowe, and M. A. Norell. 2013. Evolutionary origins of the avian brain. *Nature* **501**:93–96.

Balanoff, A. M., G. S. Bever, and M. A. Norell. 2014. Reconsidering the avian nature of the Oviraptorosaur brain (Dinosauria: Theropoda). *PLoS ONE* **9**:e113559.

Bapst, D. W. 2014. Assessing the effect of time-scaling methods on phylogeny-based analyses in the fossil record. *Paleobiology* **40**:331–351.

Baron, M. G., and P. M. Barrett. 2017. A dinosaur missing-link? *Chilesaurus* and the early evolution of ornithischian dinosaurs. *Biology Letters* **13**:20170220.

Bates, K. T., R. B. J. Benson, and P. L. Falkingham. 2012. A computational analysis of locomotor anatomy and body mass evolution in Allosauroidea (Dinosauria: Theropoda). *Paleobiology* **38**:486–507.

Benson, R. B. J. 2018. Dinosaur macroevolution and macroecology. *Annual Review of Ecology, Evolution, and Systematics* **49**:379–408.

Benson, R. B. J., N. E. Campione, M. T. Carrano, P. D. Mannion, C. Sullivan, P. Upchurch, and D. C. Evans. 2014. Rates of dinosaur body mass evolution indicate 170 million years of sustained ecological innovation on the avian stem lineage. *PLoS Biology* **12**:e1001853.

Benson, R. B. J., G. Hunt, M. T. Carrano, and N. Campione. 2018. Cope's rule and the adaptive landscape of dinosaur body size evolution. *Palaeontology* **61**:13–48.

Biewener, A. A. 1983. Allometry of quadrupedal locomotion: the scaling of duty factor, bone curvature and limb orientation to body. *Journal of Experimental Biology* **105**:147–171.

Biewener, A. A. 1989. Mammalian terrestrial locomotion and size. *BioScience* **39**:776–783.

Bishop, P. J., S. A. Hocknull, C. J. Clemente, J. R. Hutchinson, A. A. Farke, R. S. Barrett, and D. G. Lloyd. 2018a. Cancellous bone and theropod dinosaur locomotion. Part III—Inferring posture and locomotor biomechanics in extinct theropods, and its evolution on the line to birds. *PeerJ* **6**:e5777.

Bishop, P. J., S. A. Hocknull, C. J. Clemente, J. R. Hutchinson, A. A. Farke, B. R. Beck, R. S. Barrett, and D. G. Lloyd. 2018b. Cancellous bone and theropod dinosaur locomotion. Part I—an examination of cancellous bone architecture in the hindlimb bones of theropods. *PeerJ* **6**:e5778.

Bishop, P. J., K. T. Bates, V. R. Allen, D. M. Henderson, M. Randau, and J. R. Hutchinson. 2020. Relationships of mass properties and body proportions to locomotor habit in terrestrial Archosauria. *Paleobiology* **46**:550–568.

Bishop, P. J., A. Falisse, F. De Groote, and J. R. Hutchinson. 2021. Predictive simulations of running gait reveal a critical dynamic role for the tail in bipedal dinosaur locomotion. *Science Advances* **7**:eabi7348.

Bishop, P. J., C. J. Clemente, R. E. Weems, D. F. Graham, L. P. Lamas, J. R. Hutchinson, J. Rubenson, *et al.* 2017. Using step width to compare

locomotor biomechanics between extinct, non-avian theropod dinosaurs and modern obligate bipeds. *Journal of the Royal Society Interface* **14**:20170276.

Blomberg, S. P., T. Garland JR., and A. R. Ives. 2003. Testing for phylogenetic signal in comparative data: behavioral traits are more labile. *Evolution* **57**:717–745.

Bonaparte, J. F., F. E. Novas, and Coria R. A. 1990. *Carnotaurus sestrei* Bonaparte, the horned, lightly built carnosaur from the middle Cretaceous of Patagonia. *Natural History Museum of Los Angeles Contributions in Science*, no. 416, 1–42.

Botton-Divet, L. 2017. The form-function relationships in the process of secondary adaptation to an aquatic life: the contribution of semi-aquatic mammals. Ph.D. dissertation. Sorbonne Paris Cité. 254 p.

Botton-Divet, L., A. Houssaye, A. Herrel, A.-C. Fabre, and R. Cornette. 2015. Tools for quantitative form description; an evaluation of different software packages for semi-landmark analysis. *PeerJ* **3**:e1417.

Botton-Divet, L., R. Cornette, A.-C. Fabre, A. Herrel, and A. Houssaye. 2016. Morphological analysis of long bones in semi-aquatic mustelids and their terrestrial relatives. *Integrative and Comparative Biology* **56**:1298–1309.

Brusatte, S. L., and T. D. Carr. 2016. The phylogeny and evolutionary history of tyrannosauroid dinosaurs. *Scientific Reports* **6**:20252.

Brusatte, S. L., and P. C. Sereno. 2008. Phylogeny of Allosauroidea (Dinosauria: Theropoda): comparative analysis and resolution. *Journal of Systematic Palaeontology* **6**:155–182.

Brusatte, S. L., S. J. Nesbitt, R. B. Irmis, R. J. Butler, M. J. Benton, and M. A. Norell. 2010. The origin and early radiation of dinosaurs. *Earth-Science Reviews* **101**:68–100.

Brusatte, S. L., G. T. Lloyd, S. C. Wang, and M. A. Norell. 2014. Gradual assembly of avian body plan culminated in rapid rates of evolution across the dinosaur-bird transition. *Current Biology* **24**:2386–2392.

Campione, N. E. 2016. MASSTIMATE: body mass estimation equations for vertebrates, Version 2.0. https://CRAN.R-project.org/package=MASSTIMATE.

Campione, N. E., and D. C. Evans. 2012. A universal scaling relationship between body mass and proximal limb bone dimensions in quadrupedal terrestrial tetrapods. *BMC Biology* **10**:60.

Campione, N. E., and D. C. Evans. 2020. The accuracy and precision of body mass estimation in non-avian dinosaurs. *Biological Reviews* **95**:1759–1797.

Campione, N. E., D. C. Evans, C. M. Brown, and M. T. Carrano. 2014. Body mass estimation in non-avian bipeds using a theoretical conversion to quadruped stylopodial proportions. *Methods in Ecology and Evolution* **5**:913–923.

Canale, J. I., F. E. Novas, and D. Pol. 2015. Osteology and phylogenetic relationships of *Tyrannotitan chubutensis* Novas, de Valais, Vickers-Rich and Rich, 2005 (Theropoda: Carcharodontosauridae) from the Lower Cretaceous of Patagonia, Argentina. *Historical Biology* **27**:1–32.

Canale, J. I., S. Apesteguía, P. A. Gallina, J. Mitchell, N. D. Smith, T. M. Cullen, A. Shinya, A. Haluza, F. A. Gianechini, and P. J. Makovicky. 2022. New giant carnivorous dinosaur reveals convergent evolutionary trends in theropod arm reduction. *Current Biology* **32**:3195–3202.

Carrano, M. T. 1998. Locomotion in non-avian dinosaurs: integrating data from hindlimb kinematics, in vivo strains, and bone morphology. *Paleobiology* **24**:450–469.

Carrano, M. T. 1999. What, if anything, is a cursor? Categories versus continua for determining locomotor habit in mammals and dinosaurs. *Journal of Zoology* **247**:29–42.

Carrano, M. T. 2000. Homoplasy and the evolution of dinosaur locomotion. *Paleobiology* **26**:489–512.

Carrano, M. T. 2001. Implications of limb bone scaling, curvature and eccentricity in mammals and non-avian dinosaurs. *Journal of Zoology* **254**:41–55.

Carrano, M. T. 2006. Body-size evolution in the Dinosauria. Pp. 225–268 *in* M. T. Carrano, R. W. Blob, T. J. Gaudin, and J. R. Wible, eds. *Amniote paleobiology: perspectives on the evolution of mammals, birds, and reptiles*. University of Chicago Press, Chicago.

Carrano, M. T., and J. R. Hutchinson. 2002. Pelvic and hindlimb musculature of *Tyrannosaurus rex* (Dinosauria: Theropoda). *Journal of Morphology* **253**:207–228.

Carrano, M. T., and S. D. Sampson. 2008. The phylogeny of Ceratosauria (Dinosauria: Theropoda). *Journal of Systematic Palaeontology* **6**:183–236.

Carrano, M. T., S. D. Sampson, and C. A. Forster. 2002. The osteology of *Masiakasaurus knopfleri*, a small abelisauroid (Dinosauria: Theropoda) from the Late Cretaceous of Madagascar. *Journal of Vertebrate Paleontology* **22**:510–534.

Carrano, M. T., R. B. J. Benson, and S. D. Sampson. 2012. The phylogeny of Tetanurae (Dinosauria: Theropoda). *Journal of Systematic Palaeontology* **10**:211–300.

Chan, N. R. 2017. Phylogenetic variation in hind-limb bone scaling of flightless theropods. *Paleobiology* **43**:129–143.

Charig, A. J. 1972. The evolution of the archosaur pelvis and hindlimb: an explanation in functional terms. *Studies in Vertebrate Evolution* :121–155.

Chiappe, L., M. Norell, and J. Clark. 1997. *Mononykus* and birds: methods and evidence. *The Auk* **114**:300–302.

Chinsamy, A., W. D. Handley, and T. H. Worthy. 2023. Osteohistology of *Dromornis stirtoni* (Aves: Dromornithidae) and the biological implications of the bone histology of the Australian mihirung birds. *Anatomical Record* **306**:1842–1863.

Christiansen, P. 1998. Strength indicator values of theropod long bones, with comments on limb proportions and cursorial potential. *Gaia* **15**:241–255.

Christiansen, P. 1999. Scaling of the limb long bones to body mass in terrestrial mammals. *Journal of Morphology* **239**:167–190.

Cignoni, P., M. Callieri, M. Corsini, M. Dellepiane, F. Ganovelli, and G. Ranzuglia. 2008. MeshLab: an open-source mesh processing tool. Eurographics Association. http://dx.doi.org/10.2312/LocalChapterEvents/ItalChap/ItalianChapConf2008/129-136.

Clark, J. M., M. A. Norell, and R. Barsbold. 2001. Two new oviraptorids (Theropoda: Oviraptorosauria), Upper Cretaceous Djadokhta Formation, Ukhaa Tolgod, Mongolia. *Journal of Vertebrate Paleontology* **21**:209–213.

Coombs, W. P. 1978. Theoretical aspects of cursorial adaptations in dinosaurs. *Quarterly Review of Biology* **53**:393–418.

Cuesta, E., F. Ortega, and J. L. Sanz. 2018. Appendicular osteology of *Concavenator corcovatus* (Theropoda: Carcharodontosauridae) from the Lower Cretaceous of Spain. *Journal of Vertebrate Paleontology* **38**:1–24.

Cuff, A. R., O. E. Demuth, K. Michel, A. Otero, R. Pintore, D. T. Polet, A. L. A. Wiseman, and J. R. Hutchinson. 2022. Walking—and running and jumping—with dinosaurs and their cousins, viewed through the lens of evolutionary biomechanics. *Integrative and Comparative Biology* :icac049.

Cullen, T. M., J. I. Canale, S. Apesteguía, N. D. Smith, D. Hu, and P. J. Makovicky. 2020. Osteohistological analyses reveal diverse strategies of theropod dinosaur body-size evolution. *Proceedings of the Royal Society of London B* **287**:20202258.

Deeming, D. C., and G. F. Birchard. 2009. Why were extinct gigantic birds so small? *Avian Biology Research* **1**:187–194.

D'Emic, M. D., K. M. Melstrom, and D. R. Eddy. 2012. Paleobiology and geographic range of the large-bodied Cretaceous theropod dinosaur *Acrocanthosaurus atokensis*. *Palaeogeography, Palaeoclimatology, Palaeoecology* **333–334**:13–23.

D'Emic, M. D., P. M. O'Connor, R. S. Sombathy, I. Cerda, T. R. Pascucci, D. Varricchio, D. Pol, A. Dave, R. A. Coria, and K. A. Curry Rogers. 2023. Developmental strategies underlying gigantism and miniaturization in non-avialan theropod dinosaurs. *Science* **379**:811–814.

Díez Díaz, V., H. Mallison, P. Asbach, D. Schwarz, and A. Blanco. 2021. Comparing surface digitization techniques in palaeontology using visual perceptual metrics and distance computations between 3D meshes. *Palaeontology* **64**:179–202.

Egawa, S., C. T. Griffin, P. J. Bishop, R. Pintore, H. P. Tsai, J. F. Botelho, D. Smith-Paredes, *et al.* 2022. The dinosaurian femoral head experienced a morphogenetic shift from torsion to growth along the avian stem. *Proceedings of the Royal Society of London B* **289**:20220740.

Etienne, C., A. Filippo, R. Cornette, and A. Houssaye. 2021. Effect of mass and habitat on the shape of limb long bones: A morpho-functional investigation on Bovidae (Mammalia: Cetartiodactyla). *Journal of Anatomy* **238**:886–904.

Ezcurra, M. D. 2006. A review of the systematic position of the dinosauriform archosaur *Eucoelophysis baldwini* Sullivan & Lucas, 1999 from the Upper Triassic of New Mexico, USA. *Geodiversitas* **28**:649–684.

Fabbri, M., G. Navalón, R. B. J. Benson, D. Pol, J. O'Connor, B.-A. S. Bhullar, G. M. Erickson, M. A. Norell, *et al.* 2022. Subaqueous foraging among carnivorous dinosaurs. *Nature* **603**:852–857.

https://doi.org/10.1017/pab.2024.6 Published online by Cambridge University Press

Falkingham, P. 2012. Acquisition of high resolution three-dimensional models using free, open-source, photogrammetric software. *Palaeontologia Electronica* **15**.

Farlow, J. O., S. M. Gatesy, T. R. Holtz, J. R. Hutchinson, and J. M. Robinson. 2000. Theropod locomotion. *American Zoologist* **40**:640–663.

Fau, M., R. Cornette, and A. Houssaye. 2016. Photogrammetry for 3D digitizing bones of mounted skeletons: potential and limits. *Comptes Rendus Palevol* **15**:968–977.

Funston, G. 2020. Caenagnathids of the Dinosaur Park Formation (Campanian) of Alberta, Canada: anatomy, osteohistology, taxonomy, and evolution. *Vertebrate Anatomy Morphology Palaeontology* **8**:105–153.

Gatesy, S. M. 1990. Caudofemoral musculature and the evolution of theropod locomotion. *Paleobiology* **16**:170–186.

Gatesy, S. M. 1991. Hind limb scaling in birds and other theropods: implications for terrestrial locomotion. *Journal of Morphology* **209**:83–96.

Gatesy, S. M., and K. M. Middleton. 1997. Bipedalism, flight, and the evolution of theropod locomotor diversity. *Journal of Vertebrate Paleontology* **17**:308–329.

Gauthier, J. 1986. Saurischian monophyly and the origin of birds. *Memoirs of the California Academy of Sciences* **8**:1–55.

Goswami, A., A. Watanabe, R. N. Felice, C. Bardua, A.-C. Fabre, and P. D. Polly. 2019. High-density morphometric analysis of shape and integration: the good, the bad, and the not-really-a-problem. *Integrative and Comparative Biology* **59**:669–683.

Gower, J. C. 1975. Generalized Procrustes analysis. *Psychometrika* **40**:33–51.

Gregory, W. K. 1912. Notes on the principles of quadrupedal locomotion and on the mechanism of the limbs in hoofed animals. *Annals of the New York Academy of Sciences* **22**:267–294.

Grillo, O. N., and R. Delcourt. 2017. Allometry and body length of abelisauroid theropods: *Pycnonemosaurus nevesi* is the new king. *Cretaceous Research* **69**:71–89.

Gunz, P., and P. Mitteroecker. 2013. Semilandmarks: a method for quantifying curves and surfaces. *Hystrix* **24**:103–109.

Gunz, P., P. Mitteroecker, and F. L. Bookstein. 2005. Semilandmarks in three dimensions. Pp. 73–98 *in* D. E. Slice, ed. *Modern morphometrics in physical anthropology*. Kluwer Academic/Plenum, New York.

Gunz, P., P. Mitteroecker, S. Neubauer, G. W. Weber, and F. L. Bookstein. 2009. Principles for the virtual reconstruction of hominin crania. *Journal of Human Evolution* **57**:48–62.

Harris, J. D. 1998. A reanalysis of *Acrocanthosaurus atokensis*, its phylogenetic status, and paleobiogeographic implications, based on a new specimen from Texas. *New Mexico Museum of Natural History and Science Bulletin* 13.

Hedrick, B. P., E. R. Schachner, G. Rivera, P. Dodson, and S. E. Pierce. 2019. The effects of skeletal asymmetry on interpreting biologic variation and taphonomy in the fossil record. *Paleobiology* **45**:154–166.

Hedrick, B. P., B. V. Dickson, E. R. Dumont, and S. E. Pierce. 2020. The evolutionary diversity of locomotor innovation in rodents is not linked to proximal limb morphology. *Scientific Reports* **10**:717.

Hildebrand, M. 1974. *Circulatory system. In Analysis of vertebrate structure*. Wiley, New York, pp. 261–275.

Hocknull, S. A., M. A. White, T. R. Tischler, A. G. Cook, N. D. Calleja, T. Sloan, and D. A. Elliott. 2009. New mid-Cretaceous (Latest Albian) dinosaurs from Winton, Queensland, Australia. *PLoS ONE* **4**:e6190.

Holtz, T. R. 1994. The phylogenetic position of the Tyrannosauridae: implications for theropod systematics. *Journal of Paleontology* **68**:1100–1117.

Holtz, T. R., and H. Osmólska. 2004. Saurischia. Pp. 21–24 *in* D. B. Weishampel, P. Dodson and H. Osmolska, eds. *The Dinosauria*, 2nd ed. University of California Press, Berkeley.

Holtz, T. R., R. E. Molnar, and P. J. Currie. 2004. Basal Tetanurae. Pp. 71–110 *in* D. B. Weishampel, P. Dodson and H. Osmolska, eds. *The Dinosauria*, 2nd ed. University of California Press, Berkeley.

Hone, D., and T. Holtz. 2021. Evaluating the ecology of *Spinosaurus*: shoreline generalist or aquatic pursuit specialist? *Palaeontologia Electronica* **24**:a03.

Houssaye, A., K. Waskow, S. Hayashi, R. Cornette, A. H. Lee, and J. R. Hutchinson. 2016. Biomechanical evolution of solid bones in large animals: a microanatomical investigation. *Biological Journal of the Linnean Society* **117**:350–371.

Houssaye, A., F. Martin, J.-R. Boisserie, and F. Lihoreau. 2021. Paleoecological inferences from long bone microanatomical specializations in Hippopotamoidea (Mammalia, Artiodactyla). *Journal of Mammalian Evolution* **28**:847–870.

Hutchinson, J. R. 2001. The evolution of femoral osteology and soft tissues on the line to extant birds (Neornithes). *Zoological Journal of the Linnean Society* **131**:169–197.

Hutchinson, J. R. 2021. The evolutionary biomechanics of locomotor function in giant land animals. *Journal of Experimental Biology* **224**: jeb217463.

Hutchinson, J. R., and V. Allen. 2009. The evolutionary continuum of limb function from early theropods to birds. *Naturwissenschaften* **96**:423–448.

Hutchinson, J. R., and S. M. Gatesy. 2000. Adductors, abductors, and the evolution of archosaur locomotion. *Paleobiology* **26**:734–751.

Ibrahim, N., P. C. Sereno, C. Dal Sasso, S. Maganuco, M. Fabbri, D. M. Martill, S. Zouhri, N. Myhrvold, and D. A. Iurino. 2014. Semiaquatic adaptations in a giant predatory dinosaur. *Science* **345**:1613–1616.

Ibrahim, N., S. Maganuco, C. Dal Sasso, M. Fabbri, M. Auditore, G. Bindellini, D. M. Martill, *et al.* 2020. Tail-propelled aquatic locomotion in a theropod dinosaur. *Nature* **581**:67–70.

Irmis, R. B. 2011. Evaluating hypotheses for the early diversification of dinosaurs. *Earth and Environmental Science Transactions of the Royal Society of Edinburgh* **101**:397–426.

Keitt, T. H. 2008. Coherent ecological dynamics induced by large-scale disturbance. *Nature* **454**:331–334.

Klingenberg, C. P. 2016. Size, shape, and form: concepts of allometry in geometric morphometrics. *Development Genes and Evolution* **226**:113–137.

Kubo, T., and M. O. Kubo. 2012. Associated evolution of bipedality and cursoriality among Triassic archosaurs: a phylogenetically controlled evaluation. *Paleobiology* **38**:474–485.

Kundrát, M. 2007. Avian-like attributes of a virtual brain model of the oviraptorid theropod *Conchoraptor gracilis*. *Die Naturwissenschaften* **94**:499–504.

Lee, M. S. Y., A. Cau, D. Naish, and G. J. Dyke. 2014. Sustained miniaturization and anatomical innovation in the dinosaurian ancestors of birds. *Science* **345**:562–566.

Lefebvre, R., R. Allain, A. Houssaye, and R. Cornette. 2020. Disentangling biological variability and taphonomy: shape analysis of the limb long bones of the sauropodomorph dinosaur *Plateosaurus*. *PeerJ* **8**:e9359.

Lefebvre, R., A. Houssaye, H. Mallison, R. Cornette, and R. Allain. 2022. A path to gigantism: three-dimensional study of the sauropodomorph limb long bone shape variation in the context of the emergence of the sauropod bauplan. *Journal of Anatomy* **24**:297–336.

Maddison, W. P., and D. R. Maddison. 2019. Mesquite: a modular system for evolutionary analysis. [Freeware]

Maidment, S. C. R., and P. M. Barrett. 2012. Does morphological convergence imply functional similarity? A test using the evolution of quadrupedalism in ornithischian dinosaurs. *Proceedings of the Royal Society of London B* **279**:3765–3771.

Mallet, C., R. Cornette, G. Billet, and A. Houssaye. 2019. Interspecific variation in the limb long bones among modern rhinoceroses—extent and drivers. *PeerJ* **7**:e7647.

Mallet, C., G. Billet, R. Cornette, and A. Houssaye. 2022. Adaptation to graviportality in Rhinocerotoidea? An investigation through the long bone shape variation in their hindlimb. *Zoological Journal of the Linnean Society* **196**:1235–1271.

Martinelli, A. G., T. S. Marinho, F. B. Egli, E. M. Hechenleitner, F. V. Iori, F. H. Veiga, G. Basilici, M. V. T. Soares, A. Marconato, and L. C. B. Ribeiro. 2019. Noasaurid theropod (Abelisauria) femur from the Upper Cretaceous Bauru Group in Triângulo Mineiro (southeastern Brazil). *Cretaceous Research* **104**:104181.

Martín-Serra, A., B. Figueirido, and P. Palmqvist. 2014. A three-dimensional analysis of the morphological evolution and locomotor behaviour of the carnivoran hind limb. *BMC Evolutionary Biology* **14**:129.

Mazzetta, G. V., R. A. Fariña, and S. F. Vizcaíno. 1998. On the palaeobiology of the South American horned theropod *Carnotaurus sastrei* Bonaparte. *Gaia* **185**:192.

https://doi.org/10.1017/pab.2024.6 Published online by Cambridge University Press

McPhee, B. W., R. B. J. Benson, J. Botha-Brink, E. M. Bordy, and J. N. Choiniere. 2018. A giant dinosaur from the earliest Jurassic of South Africa and the transition to quadrupedality in early sauropodomorphs. *Current Biology* **28**:3143–3151.e7.

Mitteroecker, P., and P. Gunz. 2009. Advances in geometric morphometrics. *Evolutionary Biology* **36**:235–247.

Novas, F. E. 1996. Dinosaur monophyly. *Journal of Vertebrate Paleontology* **16**:723–741.

Novas, F. E., M. D. Ezcurra, F. L. Agnolin, D. Pol, and R. Ortíz. 2012. New Patagonian Cretaceous theropod sheds light about the early radiation of Coelurosauria. *Revista del Museo Argentino de Ciencias Naturales* **14**:57–81.

Novas, F. E., L. Salgado, M. Suárez, F. L. Agnolín, M. D. Ezcurra, N. R. Chimento, R. de la Cruz, M. P. Isasi, A. O. Vargas, and D. Rubilar-Rogers. 2015. An enigmatic plant-eating theropod from the Late Jurassic period of Chile. *Nature* **522**:331–334.

Ostrom, J. H. 1976. *Archaeopteryx* and the origin of birds. *Biological Journal of the Linnean Society* **8**:91–182.

Padian, K., and L. M. Chiappe. 1998. The origin and early evolution of birds. *Biological Reviews* **73**:1–42.

Padian, K., A. J. de Ricqlès, and J. R. Horner. 2001. Dinosaurian growth rates and bird origins. *Nature* **412**:405-408. https://doi.org/10.1038/35086500

Paradis, E., J. Claude, and K. Strimmer. 2004. APE: analyses of phylogenetics and evolution in R language. *Bioinformatics* **20**:289–290.

Parrish, J. M. 1986. Locomotor adaptations in the hindlimb and pelvis of the Thecodontia. *Hunteria* **1**:1.

Persons, W. S., and P. J. Currie. 2011. Dinosaur speed demon: the caudal musculature of *Carnotaurus sastrei* and implications for the evolution of South American Abelisaurids. *PLoS ONE* **6**:e25763.

Pintore, R., A. Delapré, R. Lefebvre, L. Botton-Divet, A. Houssaye, and R. Cornette. 2022a. The potential and limits of thin-plate spline retrodeformation on asymmetrical objects: simulation of taphonomic deformations and application on a fossil sample of limb long bones. *Comptes Rendus Palevol* **21**:191–205.

Pintore, R., A. Houssaye, S. J. Nesbitt, and J. R. Hutchinson. 2022b. Femoral specializations to locomotor habits in early archosauriforms. *Journal of Anatomy* **240**:867–892.

Polly, P. D. 2007. Limbs in mammalian evolution. Pp. 245–268 *in* B. K. Hall, ed. *Fins into limbs: evolution, development, and transformation*. University of Chicago Press, Chicago.

Rohlf, F. J., and D. Slice. 1990. Extensions of the Procrustes method for the optimal superimposition of landmarks. *Systematic Biology* **39**: 40–59.

Schlager, S. 2017. Morpho and Rvcg—shape analysis in R. Pp. 217–256 *in* G. Zheng, S. Li, and G. Szekely, eds. *Statistical shape and deformation analysis*. Elsevier, Amsterdam.

Sereno, P. C. 1999. The evolution of dinosaurs. *Science* **284**:2137–2147.

Sereno, P. C., R. N. Martínez, and O. A. Alcober. 2012. Osteology of *Eoraptor lunensis* (Dinosauria, Sauropodomorpha). *Journal of Vertebrate Paleontology* **32**:83–179.

Sereno, P. C., N. Myhrvold, D. M. Henderson, F. E. Fish, D. Vidal, S. L. Baumgart, T. M. Keillor, K. K. Formoso, and L. L. Conroy. 2022. Spinosaurus is not an aquatic dinosaur. *eLife* **11**:e80092.

Soodmand, E., D. Kluess, P. A. Varady, R. Cichon, M. Schwarze, D. Gehweiler, F. Niemeyer, D. Pahr, and M. Woiczinski. 2018. Interlaboratory comparison of femur surface reconstruction from CT data compared to reference optical 3D scan. *BioMedical Engineering OnLine* **17**:29.

Sookias, R. B., R. J. Butler, and R. B. J. Benson. 2012. Rise of dinosaurs reveals major body-size transitions are driven by passive processes of trait evolution. *Proceedings of the Royal Society of London B* **279**:2180–2187.

Tsai, H. P., K. M. Middleton, J. R. Hutchinson, and C. M. Holliday. 2018. Hip joint articular soft tissues of non-dinosaurian Dinosauromorpha and early Dinosauria: evolutionary and biomechanical implications for Saurischia. *Journal of Vertebrate Paleontology* **38**:e1427593.

Tsai, H. P., K. M. Middleton, J. R. Hutchinson, and C. M. Holliday. 2020. More than one way to be a giant: convergence and disparity in the hip joints of saurischian dinosaurs. *Evolution* **74**:1654–1681.

Turner, A. H., D. Pol, J. A. Clarke, G. M. Erickson, and M. A. Norell. 2007. A basal dromaeosaurid and size evolution preceding avian flight. *Science* **317**:1378–1381.

Turner, A. H., P. J. Makovicky, and M. A. Norell. 2012. A review of dromaeosaurid systematics and paravian phylogeny. *Bulletin of the American Museum of Natural History* **2012**:1–206.

Tykoski, R. S., and T. Rowe. 2004. Ceratosauria. Pp. 47–70 *in* D. B. Weishampel, P. Dodson and H. Osmolska, eds. *The Dinosauria*, 2nd ed. University of California Press, Berkeley.

Waltenberger, L., K. Rebay-Salisbury, and P. Mitteroecker. 2021. Three-dimensional surface scanning methods in osteology: a topographical and geometric morphometric comparison. *American Journal of Physical Anthropology* **174**:846–858.

Wiley, D. F., N. Amenta, D. A. Alcantara, D. Ghosh, Y. J. Kil, E. Delson, W. Harcourt-Smith, F. J. Rohlf, K. St John, and B. Hamann. 2005. Evolutionary morphing. IS 05. *IEEE Visualization* **2005**:431–438. https://doi.org/10.1109/VISUAL.2005.1532826.

Wynd, B. M., J. C. Uyeda, and S. J. Nesbitt. 2021. Including distorted specimens in allometric studies: linear mixed models account for deformation. *Integrative Organismal Biology* **3**:obab017.

Xu, X., and M. A. Norell. 2004. A new troodontid dinosaur from China with avian-like sleeping posture. *Nature* **431**:838–841.

Zanno, L. E., and P. J. Makovicky. 2013. No evidence for directional evolution of body mass in herbivorous theropod dinosaurs. *Proceedings of the Royal Society of London B* **280**:20122526.

Zelditch, M., D. Swiderski, and H. D. Sheets. 2012. *Geometric morphometrics for biologists: a primer*. Elsevier/Academic Press, London.

https://doi.org/10.1017/pab.2024.6 Published online by Cambridge University Press